Desalination and Water Treatment
www.deswater.com
doi: 10.5004/dwt.2023.30074

312 (2023) 139–157
November

Adsorptive removal of boron from aqueous solutions using peels of jering seeds (*Archidendron pauciflorum*): isotherm, kinetic and thermodynamic studies

Fawaz Al-Badaii[a,b], Riyadh Abdulmalek Hassan[c,d], Nurul 'Ain Abdul Jalil[a], Azhar Abdul Halim[a,*]

[a]*Department of Earth Sciences and Environment, Faculty of Science and Technology, Universiti Kebangsaan Malaysia, 43600 UKM Bangi, Selangor, Malaysia, emails: azharhalim@ukm.edu.my (A.A. Halim), fawaz.albadai@tu.edu.ye (F. Al-Badaii), nurulain@ukm.edu.my (N.A. Abdul Jalil)*
[b]*Biology Department, Faculty of Applied Science, Thamar University, Dhamar 87246, Yemen*
[c]*Department of Chemical Sciences, Faculty of Science and Technology, Universiti Kebangsaan Malaysia, Bangi 43600, Selangor, Malaysia, email: rydh1974@yahoo.com (R.A. Hassan)*
[d]*Department of Chemistry, Faculty of Science, Ibb University, P.O. Box: 70270, Ibb, Yemen*

Received 18 June 2023; Accepted 3 October 2023

ABSTRACT

The excessive presence of boron in the environment due to extensive industrial use can severely affect the ecosystem and human health, leading to health problems associated with skin and eye irritation, respiratory issues, and gastrointestinal disorders in humans. Therefore, this study investigated the potential of jering seed peels as an adsorbent for removing boron from aqueous solutions. The batch system was used to evaluate the efficiency of raw jering adsorbent (RJA), modified jering adsorbent by $FeCl_3$ (MJA1), and modified jering adsorbent by NaOH (MJA2) under varying conditions, including pH, initial concentration, adsorbent dose, contact time, and temperature. Analysis using Fourier-transform infrared spectroscopy, field emission scanning electron microscopy, and energy-dispersive X-ray spectroscopy was conducted to characterize the adsorbents, confirming the changes of jering adsorbents before and after the adsorption process. The optimal pH of boron removal efficiency was 6.5 for MJA1 and 7 for RJA and MJA2. The efficiency decreased with increasing initial concentration and temperature but increased with increasing adsorbent amount and contact time. The Langmuir, Freundlich, Temkin, and Dubinin–Radushkevich models were applied to study adsorption isotherm, the Langmuir isotherm model for RJA (R^2 = 0.99) and MJA1 (R^2 = 0.92) and Freundlich isotherm model for MJA2 (R^2 = 0.91) represented the measured sorption data well. Pseudo-first-order, pseudo-second-order, intraparticle diffusion, and Elovich models were applied to study adsorption kinetics that fitted best to the pseudo-second-order kinetic model for RJA (R^2 = 1.00) and MJA1 (R^2 = 0.99) and fitted best to the Elovich kinetic model for MJA2 (R^2 = 0.99). Thermodynamics was investigated, and the negative values of $\Delta H°$ and $\Delta S°$ showed that the boron adsorption is favourable, spontaneous, and exothermic and reduces system entropy as the adsorbate organizes at the solid-solute interface during the adsorption process. The jering adsorbents also showed good reusability during the initial and subsequent adsorption–desorption cycles, indicating potential recyclable adsorbents. Hence, utilizing jering adsorbents to eliminate boron from water resources can be feasible, cost-effective, and eco-friendly.

Keywords: Adsorption; *Archidendron pauciflorum*; Boron removal

* Corresponding author.

1. Introduction

Boron, a naturally occurring element found in water, rocks, and soil, plays a crucial role in plant growth in small quantities, but excessive levels can harm plants and animals [1,2]. Elevated boron concentrations in drinking water have been associated with skin irritation, gastrointestinal disorders, and reproductive issues in prolonged exposures [3]. While boron pollution originates from natural sources such as volcanic ash leaching and erosion of boron-containing rocks, human activities, including agriculture and industrial processes like mining and waste disposal, contribute significantly [4–6]. The World Health Organization (WHO) guidelines for drinking water quality recommend a provisional threshold of 2.4 mg/L for boron concentration, considering its impact on health and the viability of removal strategies [7]. Although most freshwater sources maintain lower boron levels, ranging from 0.003 to 0.337 mg/L, seawater contains notably higher concentrations of around 4–5 mg/L, surpassing WHO limits [8]. Consequently, seawater desalination necessitates additional measures to align boron levels with accepted standards [9]. The complexity of addressing boron in desalination arises from the prevalence of stable boric acid, which poses challenges to the efficacy of separation methods, including reverse osmosis membranes [10]. This intricate issue encompasses health concerns, resistance to conventional removal techniques, and ecological implications [11].

In a study conducted by Guan et al. [11], it was found that standard treatment plant systems are not successful in eliminating boron from water due to the presence of boric acid in its protonated form at low pH. This form of boron is uncharged, allowing it to permeate through reverse osmosis membranes. Multiple techniques have been identified as effective for removing boron from contaminated water and aqueous solutions. These methods include flocculation–precipitation, reverse osmosis, electrodialysis, extraction of dissolved compounds, membrane filtering, adsorption, and electrocoagulation [1,5,11,12]. Adsorption is considered a highly cost-effective approach for removing low boron concentrations, as supported by several studies [2,13–16]. Using affordable agricultural biomass, such as jering peels, as adsorbents for adsorption processes is a highly economical approach for removing boron concentrations from water due to the comparatively low cost of the adsorbents and their ability to be conveniently regenerated for further usage [17–19]. The adsorption process operates through attracting and binding boron molecules to the surface of the adsorbent material [17]. The choice of adsorbent depends on the water source's properties and the concentration of boron [6]. Several studies have demonstrated the efficacy of adsorbents such as activated carbon, zeolites, and clay minerals in removing boron from aqueous solutions. As Kluczka et al. [20] demonstrated, activated carbon exhibited significant efficacy in removing boron from water with elevated levels. Kavak [21] found comparable results, indicating that using calcined alunite was influential in removing boron from water, even at elevated quantities of up to 20 mg/L. Adsorption is easily integrated into existing water treatment systems. Additionally, this technology is characterized by its low energy consumption, rendering it more cost-effective compared to alternative methods of boron removal, such as reverse osmosis [22,23].

The potential of jering seed peels (*Archidendron pauciflorum*) as an adsorbent material for removing diverse contaminants from water has been documented in previous studies [24,25]. Jering seed peels possess characteristics that make them valuable and sustainable adsorbents, such as the significant concentration of polyphenolic chemicals, tannins, and flavonoids, which are well-documented for their adsorption capabilities [26,27]. The chemical constituents included in jering peels are accountable for the significant adsorption capability exhibited towards chemical contaminants found in water. The utilization of jering seed peels as an adsorbent material has been highly successful in removing various chemical contaminants present in water, including metal ions and dyes [24,27]. Natural, renewable, and cost-effective adsorbents can effectively eliminate substantial amounts of chemical contaminants from water, even in low quantities [27,28]. The jering seed peels exhibit promising potential as a very effective bio-adsorbent material for the removal of various pollutants from water sources that have been contaminated. This efficacy can be attributed to the significant carbon content in these peels, as supported by several studies [25,27,29,30]. Hence, it can be inferred that using adsorbent materials, such as jering seed peels, offers numerous benefits compared to conventional alternatives. These advantages encompass cost-effectiveness, enhanced efficacy, minimal chemical or biological sludge presence, and environmental sustainability adherence [30]. Boron, a naturally occurring element in water from industrial and agricultural activities, threatens human health and the environment, mainly aquatic life, due to its high-water solubility. Conventional treatment techniques, such as physical and chemical processes, often struggle to remove the element from water effectively. Consequently, the study intends to evaluate a potent alternative treatment approach, the adsorption method, for removing boron from synthetic wastewater using jering seed peels as an adsorbent.

2. Materials and methods

2.1. Materials

The chemicals used in this study were of analytical grade and purchased from Sigma-Aldrich in Malaysia, including sodium hydroxide (NaOH), ferric chloride ($FeCl_3$), hydrochloric acid (HCl), sulfuric acid (H_2SO_4), and boric acid (H_3BO_3).

2.2. Collection and preparation of the adsorbent

The current study examined the efficacy of jering seed peels as adsorbents. The jering fruits were obtained at the Central Fruit and Vegetable Market in Kajang, Malaysia. The peels underwent multiple washing cycles using distilled water to remove contaminants and were dried in an oven at 60°C for 48 h. Subsequently, the desiccated peels were pulverized utilizing a crusher. The obtained powder was subjected to sieving using a British Standard Sieve. Particles smaller than 300 μm were gathered in a plastic container. These particles were used in their original form as raw jering adsorbent (RJA) and were also subjected to

treatment to modify their properties for use in the adsorption experiments [27–29].

2.3. Modification of raw jering peels adsorbent

The chemical alteration was used to create the modified jering peel powder material. Modified jering adsorbent by $FeCl_3$ (MJA1) was created by combining 10 g of raw peel powder with 100 mL of a 0.1 M iron chloride ($FeCl_3$) solution. The modified jering adsorbent by NaOH (MJA2) was also prepared by combining 10 g of raw peel powder with 100 mL of a 0.1 M sodium hydroxide (NaOH) solution. Each of the mixtures was subjected to agitation using a magnetic stirrer for 24 h. Subsequently, the powders were filtered and thoroughly washed with distilled water before being oven-dried at 50°C for an extended period. The resultant material was then utilized as adsorbents [31,32].

2.4. Preparation and determination of adsorbate

The adsorbate used in this study was boric acid that was prepared by dissolving 5.716 g of anhydrous boric acid (H_3BO_3) from Merck Chemical Company (Supplier of Merck Chemical Company, Malaysia; Manufacturer is Germany) in deionized water, resulting in a stock solution that was then diluted to a final volume of 1,000 mL. Synthetic wastewater was prepared by diluting the stock solution to obtain the desired concentrations [1,12,33]. The Carmine method, described in the DR 2700 Spectrophotometer (HACH Company, Germany) user manual, was used to determine the boron concentration [21]. Firstly, the procedure involved the addition of 75 mL of sulfuric acid (H_2SO_4) solution to a 250 mL conical flask, followed by the addition of the Boro ver 3 boron reagent powder pillows and thorough mixing. Then, the solution was allowed to stand for 5 min to ensure the complete dissolution of the reagent powder. The experiment was conducted in a well-ventilated room using volatile, concentrated chemicals such as H_2SO_4. Then, 2 mL of the sample was transferred to a 125 mL conical flask and mixed with 35 mL of the H_2SO_4 reagent. Next, the solution was allowed to react for 25 min. Finally, at least 10 mL of the sample was transferred to a cell holder, and the boron concentration was measured using the DR 2700 Spectrophotometer (HACH Company, Germany).

2.5. Characterization of adsorbent

A Thermo Scientific Nicolet 6700-FTIR 12 Spectrometer (United States) was employed to conduct an Fourier-transform infrared spectroscopy (FTIR) analysis to determine the exterior functional groups and chemical bonds of the synthesized RJA, MJA1, and MJA2 adsorbents [20,27]. A Gemini Model 18 SUPRA 55VP-ZEISS Oberkochen (Germany) field emission scanning electron microscopy (FESEM), equipped with energy-dispersive X-ray spectroscopy (EDX), was utilized to carry out morphological surface mapping of the RJA, MJA1, and MJA2 adsorbents [28,34].

2.6. Adsorption study

The efficacy of jering peel powder as adsorbents for boron removal was assessed in a batch screening [31,33,35]. To achieve the experiment, 1 g of the adsorbent was added to 100 mL of boron solution with an initial concentration (C_0) of 15 mg/L in 250 mL Erlenmeyer flasks. The pH of the boron solution was not adjusted as it was already at the desired level, and the samples were placed in an orbital shaking incubator at 220 rpm and a temperature of 303 K. After 2 h, the samples were removed from the incubator, and filtered using 0.45 μm filter paper. The remaining boron concentration was measured at 605 nm using 2 mL of the filtered sample in a new 250 mL conical flask with the Carmine method. The adsorption capacity (q_e) and efficiency (R%) of the adsorbent were determined using Eqs. (1) and (2), respectively.

$$q_e = \frac{C_0 - C_e}{W} \times V \tag{1}$$

$$q\% = \frac{C_0 - C_e}{C_0} \times 100 \tag{2}$$

where q_e is the boron distributed on the adsorbent surface, or q_e (mg/g), and C_0 and C_e were the adsorbate's initial and final concentrations (mg/L), respectively. W and V are the adsorbent (g) mass and solution (L) volume, respectively.

Both adsorption capacity (q_e) and efficiency (R%) are crucial factors for evaluating and comparing the effectiveness of different adsorbents [19,36]. The experimental study involved conducting adsorption experiments to investigate the effects of various factors on the adsorption process. These factors included the initial solution pH (ranging from 2 to 12.5), adsorbent dose (ranging from 0.2 to 1.5 g), contact time (ranging from 10 to 120 min), initial boron concentration (ranging from 2 to 20 mg/L), and temperature (ranging from 25°C to 50°C). The study aimed to analyze the process's adsorption kinetics, adsorption isotherm, and thermodynamic aspects. The impact of operational and environmental factors on the adsorbent's batch removal capacity was investigated up to the point of equilibrium, which was determined for each specific adsorbent.

2.7. Isotherm model analysis

Langmuir, Freundlich, Temkin, and Dubinin–Radushkevich isotherm models were used in this investigation. The isotherm quantifies the creation of a monolayer adsorbate on the adsorbent's outer surface, after which no additional adsorption occurs [31,37]. The model assumes homogeneous surface adsorption energies and no adsorbate transmigration [38]. By linearly graphing $1/q_e$ vs. $1/C_e$, Eq. (3) determined the Langmuir model.

$$\frac{1}{q_e} = \frac{1}{q_{\max}} + \frac{1}{K_L q_{\max} C_e} \tag{3}$$

The equilibrium adsorbate concentration in solution is denoted by q_e, the maximum adsorption capacity is denoted by q_m, and the Langmuir constant, K_L, is denoted by L/mg.

The Freundlich adsorption isotherm model is widely used in adsorption, particularly for adsorbent materials with highly irregular surfaces. This model considers multilayer growth occurring on the surface [38]. In order to

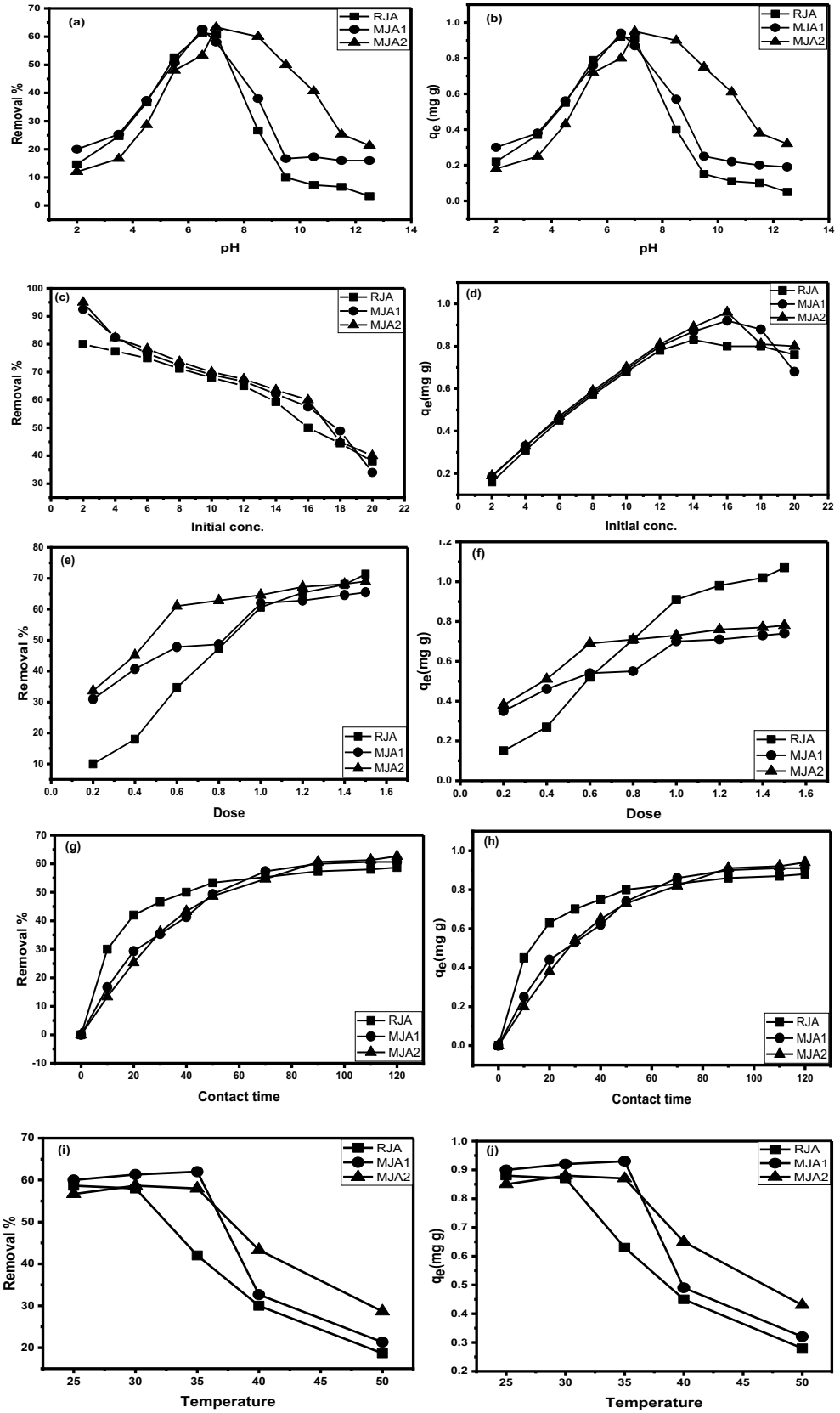

Fig. 1. Effect of pH (a,b), initial concentration (c,d), adsorbent dose (e,f), contact time (g,h), and temperature (i,j) on boron adsorption efficiency (q_e and R%) by RJA, MJA1, and MJA2. The conditions were pH 6.5, concentration of 15 mg/L, dose of 1 g, 120-min time, and temperature of 30°C.

illustrate the Freundlich model, it is necessary to create a linear plot by plotting the logarithm of q_e against the logarithm of C_e, utilizing Eq. (4).

$$\log q_e = \log K_f + \frac{1}{n}\log C_e \tag{4}$$

where $1/n$ represents the intensity of adsorption, and K_f represents adsorption capacity. The Freundlich expression's constants, K_f and $1/n$, were obtained from its linear version.

The Temkin isotherm incorporates a component that accounts for the interaction between the adsorbent and the adsorbate. The model postulates that the reduction in adsorption heat, dependent on temperature, of all molecules in the layer will follow a linear trend rather than a logarithmic trend with increasing coverage [37]. The constants were determined by plotting the slope and intercept against the natural logarithm of C_e. The equation suggests a uniform binding energy distribution up to a specific maximum binding energy. Eq. (5) represents this approach:

$$q_e = \frac{RT}{B_T}\ln A_T + \left(\frac{RT}{B_T}\right)\ln C_e \tag{5}$$

where T is the temperature, R is the universal gas constant (8.314 J/mol·K) (K), A_T (L/g) is the equilibrium binding constant, which represents the maximal bonding energy, and B_T (kJ/mol) is the heat of adsorption constant calculated from the plot of q_e in the $\ln C_e$ present.

Dubinin–Radushkevich commonly expresses the adsorption mechanism with a Gaussian energy distribution onto a heterogeneous surface [34,37]. This model has succeeded in accurately summarising data for high solute activity and intermediate concentration ranges [38]. The Dubinin–Radushkevich isotherm model uses two constants, q_{DR}, which represents the theoretical ability of the adsorbent to adsorb a single layer of sorbate in mg/g and represents the adsorption energy in mol^2/kJ^2. The Polanyi potential, expressed as J/mol, is also included, as seen in Eq. (6).

$$\ln q_e = \ln q_{DR} - \beta\varepsilon^2 \tag{6}$$

2.8. Kinetic models analysis

Adsorption kinetics are determined by the rate of equilibrium attainment, which is restricted by the mass transport mechanism and influenced by the adsorbent's and adsorbate's properties [31]. Assessing adsorption kinetics is crucial to determine the efficacy of the adsorption process [30]. The pseudo-first-order kinetic model, which is commonly used for forecasting boron adsorption kinetics [21], was presented in a linear form Eq. (7):

$$\log\left(q_e - q_t\right) = \log q_e - \left(\frac{k_1 t}{2.303}\right) \tag{7}$$

The adsorption capacity at equilibrium is denoted by q_e (mg/g), while the adsorption capacity at time t is represented by q_t (mg/g). The rate constant is denoted by k_1 (min^{-1}).

The pseudo-second-order model is utilized to evaluate chemisorption kinetics from liquid solutions through solid phase sorption [11] and is represented in a linear expression as in Eq. (8):

$$\frac{t}{q_t} = \left(\frac{1}{q_e}\right)t + \left(\frac{1}{k_2 q_e^2}\right) \tag{8}$$

The boron adsorption capacity of the jering adsorbent at time t (min) is represented by q_t (mg/g), while q_e (mg/g) is the adsorption capacity at equilibrium. The adsorption rate constant is denoted by k_2 (g/mg·min).

The intraparticle diffusion kinetic model typically explains solutes' diffusion into porous particles [37,38]. According to this model, the step that determines the rate is solute diffusion within the particle, and the solute concentration within the particle varies in direct proportion to the square root of time [22]. Eq. (9) represents this model:

$$q_t = K_{diff} t^{0.5} \times C \tag{9}$$

where q_t represents the adsorption capacity at time t, while $t^{0.5}$ represents the half-life time in seconds, the intercept C represents the starting concentration inside the porous particle, and K_{diff} (mg/g·$min^{0.5}$) represents the intraparticle diffusion rate constant.

The Elovich kinetic model is commonly employed to describe chemisorption processes, wherein a chemical reaction takes place between the adsorbate and the adsorbent surface. The proposed model assumes that the adsorption process consists of two distinct stages: an initial rapid phase known as chemisorption, followed by a subsequent slower step referred to as the diffusion of the adsorbate onto the surface [6,30]. The equation of this model is as follows:

$$q_t = \frac{1}{\alpha}\ln\left(\alpha\beta\right) + \frac{1}{\alpha}\ln t \tag{10}$$

where it represents the quantity of adsorbate adsorbed per mass of adsorbent at time t, α the initial adsorption rate (mg/g·min), β the desorption constant, and t the time.

2.9. Thermodynamic model analysis

The consideration of energy and entropy values is essential to determine which processes occur spontaneously in adsorption systems [22,39]. Analyzing thermodynamic parameters helps identify the practical application of these processes [38]. Eq. (11) can be used to calculate parameters like Gibbs free energy ($\Delta G°$, kJ/mol), enthalpy ($\Delta H°$, kJ/mol), and entropy ($\Delta S°$, J/mol·K).

$$\Delta G = -RT\ln K_a \tag{11}$$

The equation includes several parameters, including the free energy of adsorption ($\Delta G°$, kJ/mol), the temperature in Kelvin (K) denoted by T, the gas constant (R, 8.314 J/mol·K), and the sorption equilibrium constant (K_a).

$$\ln K_a = \frac{\Delta H}{RT} + \frac{\Delta S}{RT} \tag{12}$$

where ΔH refers to the heat of sorption (kJ/mol), while ΔS represents the standard entropy change (kJ/mol·K).

2.10. Regeneration studies

The potential for regeneration of jering peel adsorbents, specifically RJA, MJA1, and MJA2, was assessed using 0.1 M NaOH and 0.1 M HCl to determine the proper regeneration of each adsorbent. For RJA and MJA2, the regeneration by 0.1 M NaOH was selected, while the best regeneration of MJA1 was by 0.1 M HCl. Each adsorbent (1 g) was subjected to an adsorption experiment in which it was introduced into 100 mL of synthetic aqueous solutions containing 15 mg/L boron. The amount of boron adsorbed was noted, and the adsorbent was then dried in the oven at 105°C for 12 h. Each adsorbent was separately soaked in 100 mL of 0.1 M NaOH and 0.1 M HCl solutions, followed by centrifugation at 5,000 rpm for 15 min. Subsequently, the adsorbent underwent a rinsing process utilizing 100 mL of deionized water, followed by a 12 h drying duration at 105°C within an oven, succeeded by cooling within a desiccator. Following this, the desiccated adsorbent was employed in a successive adsorption experiment. This cyclic procedure was iterated thrice for each distinct adsorbent. [40–42]. A control sample composed of deionized water was employed for comparative analysis. Each iterative cycle encompassed an approximate duration of 28 h.

3. Results and discussion

3.1. Characterization of adsorbents

The RJA, MJA1, and MJA2 FTIR spectra data reveal details about the functional groups in the adsorbent samples, as shown in Fig. 2. The stretching vibrations of the O–H and C–H bonds in the hydroxyl and methyl groups, respectively, are represented by the peaks at 3,303.43 and 2,923.7 cm^{-1} in the RJA, MJA1, and MJA2, respectively. These peaks are typical of carbohydrates, in large quantities in jering peels. The hydroxyl group is frequently found in organic substances, such as phenols, alcohols, and carbohydrates [29]. The amide group in proteins exhibits the C=O stretching vibration, represented by the peak at 1,607.46 cm^{-1} in RJA, indicating that the protein content may have been decreased during the modification process; this peak is absent in MJA1 and MJA2. The aromatic C=C stretching vibrations in the lignin of samples are represented by the peaks at 1,517.5 and 1,443.16 cm^{-1} in RJA. The stretching vibrations of the Fe–OH or Fe–O bond and the bending vibrations of the C–H bond in the aromatic ring are represented by the peaks at 3,848 and 1,447.15 cm^{-1} in MJA1. These peaks show that the modified jering powder contains $FeCl_3$. In jering powder, a coordination link between $FeCl_3$ and the nitrogen of the pyridine ring has formed [43,44], as evidenced by the 2,164 cm^{-1} peak ascribed to C≡N's stretching vibration in the pyridine ring [25]. The stretching vibrations of the N–H bond in the amine group are responsible for the MJA2 peaks at 3,738 cm^{-1}, while the bending vibrations of the C–H bonds in CH_3 groups are responsible for the peak at 1,422 cm^{-1}. The distinctive peaks for RJA, MJA1, and MJA2 are found at 1,365.32; 1,370 and 1,370 cm^{-1}, respectively. The bending vibrations of the C–H bonds in the methyl and methylene groups found in the samples are responsible for these peaks [29]. Peaks are produced at 1,229.89 cm^{-1} for RJA and 1,230 cm^{-1} for MJA1 and MJA2 by the stretching vibrations of the C–O bonds in the polysaccharides of the adsorbents. The stretching vibrations of the C–OH and C–N bonds in the glycosidic linkage in cellulose and hemicellulose, as well as in the amide groups, respectively, are linked to the peaks at 1,029.82 cm^{-1} in RJA and 1,031.76 cm^{-1} in MJA1 and MJA2, respectively. The MJA1 and MJA2 have slightly stronger peaks, indicating that the concentration of these components has increased due to alteration. The peak at 825.5 cm^{-1}, the C–H out-of-plane bending vibration of lignin and cellulose, was seen with a slightly higher intensity in RJA, MJA1, and MJA2, respectively, indicating a rise in their concentration following modification. The peak at 762.8 cm^{-1}, unique to the RJA, represents the C–H bending vibration of the aromatic ring in lignin, indicating a decrease in lignin content following $FeCl_3$ or NaOH alteration. Each sample has the aliphatic group's C–H and the hydroxyl groups' O–H stretch. The modified samples display new peaks when other functional groups are introduced throughout the modification procedure. For instance, the peaks in MJA1 and MJA2, respectively, at 2,164 and 2,316 cm^{-1}, show new functional groups such as amine and imine groups. The absence of the peak 762.8 cm^{-1} in the MJA1 and MJA2 resulted in changes of samples in the cellulose and hemicellulose concentration and a reduction in the lignin concentration after the modification, as represented by previous studies [27,29,30,45]. New functional groups in modified samples indicate that the modification procedure was successful, and the absence or reduction of specific peaks in changed samples can be attributed to the addition, deletion, or modification of particular functional groups [22,27].

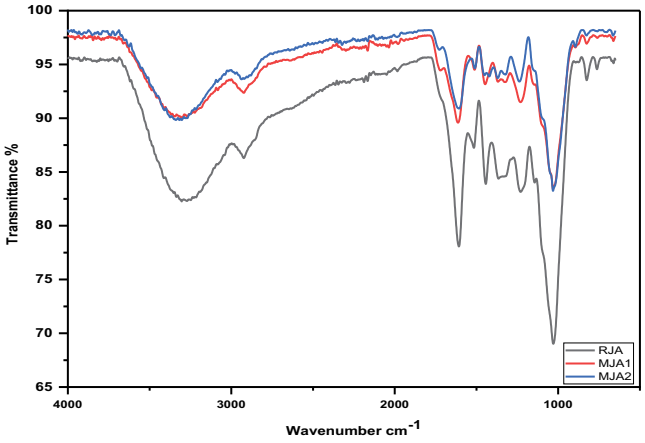

Fig. 2. Fourier-transform infrared spectroscopy transmission spectrum of RJA, MJA1, and MJA2 adsorbents in the frequency region of 500–4,000 cm^{-1} before adsorption.

FESEM was utilized to study the morphology and pore size distribution of RJA, MJA1, and MJA2 adsorbents. Fig. 3 presents the FESEM images of RJA, MJA1, and MJA2 before and after adsorption, revealing significant structural differences among the adsorbent samples. The RJA micrograph shows several pores on the surface, indicating

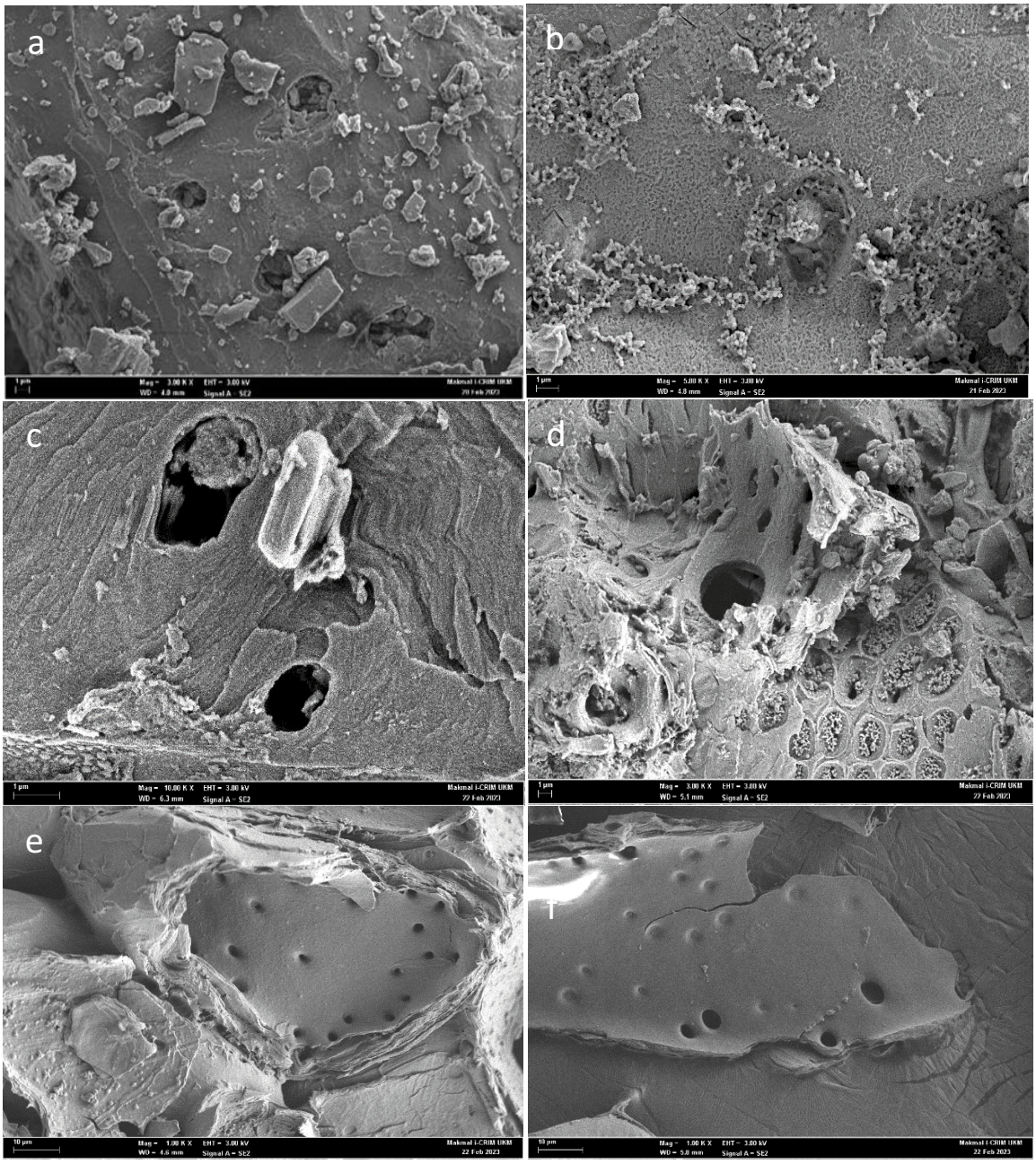

Fig. 3. Field emission scanning electron micrographs of (a) RJA before adsorption, (b) RJA after adsorption, (c) MJA1 before adsorption, (d) MJA1 after adsorption, (e) MJA2 before adsorption, and (b) MJA2 after adsorption.

its potential for boron ion uptake. The surface of RJA is relatively smooth, with irregularly shaped particles, while after adsorption, the surface became rough, with agglomerations of spherical particles covering the porous structure, confirming the adsorption. MJA1 shows clear pores before boron adsorption, but the surface becomes partially covered after exposure to boron. The micrograph of MJA2 reveals visible perforations, likely due to the leaching of structural materials, which may have exposed the active sites [46]. The modified surface of MJA1 contains pores and channels, appearing relatively rough before adsorption, but it becomes smooth, with unclear pores and lacking channels after adsorption, suggesting that the surface had been covered with an adsorbate [47]. The observed changes in the surface structure of RJA, MJA1, and MJA2 before and after boron adsorption indicate their potential application as effective adsorbents for boron removal from aqueous solutions. The elemental composition of RJA, MJA1, and MJA2 before and after boron adsorption was analyzed using EDX, as in Fig. 4. The results showed that RJA was mainly composed of carbon, oxygen, aluminium, potassium, and magnesium before boron adsorption. After adsorption, a significant decrease in carbon and oxygen content and a slight increase in potassium content were observed, indicating the

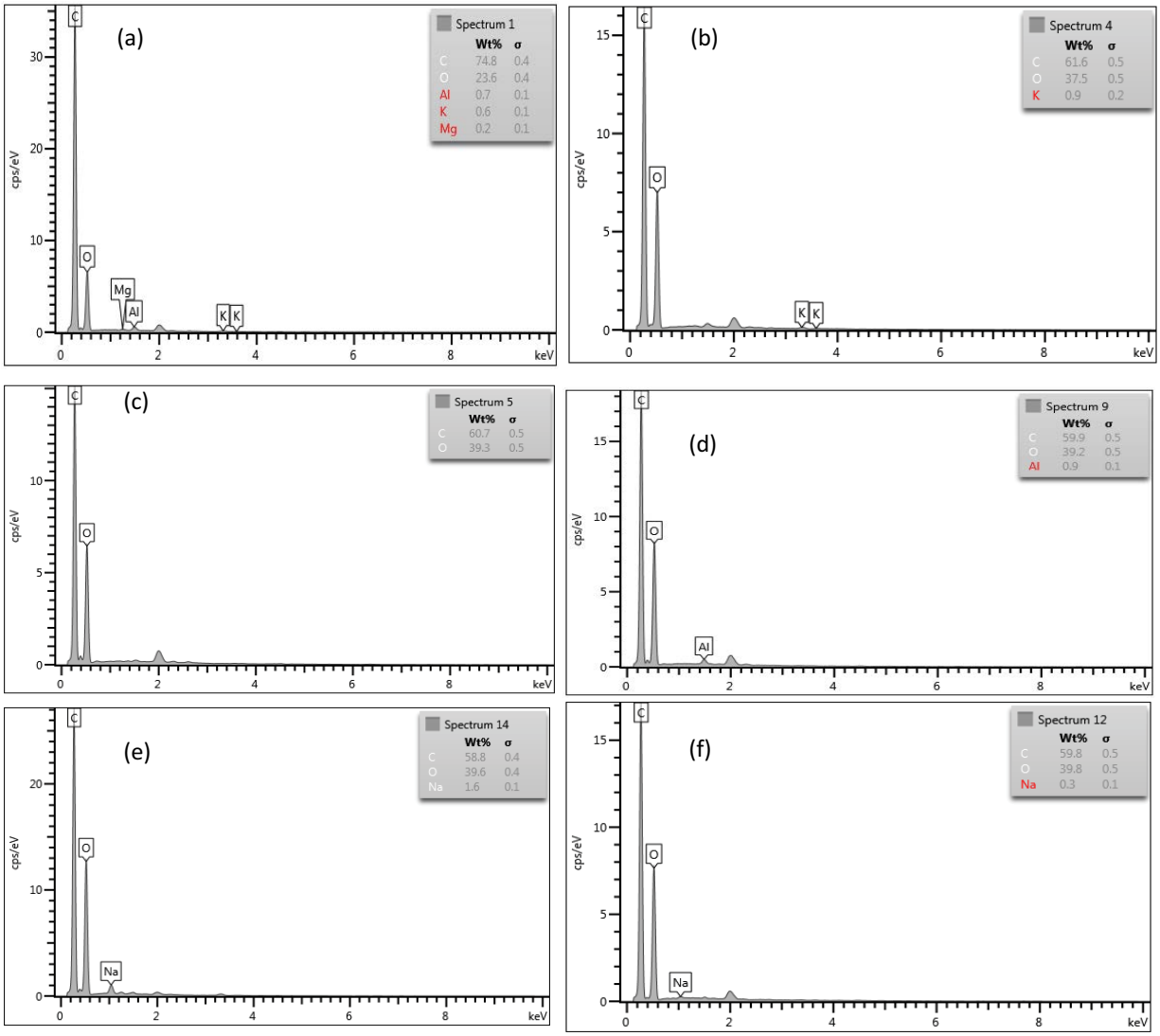

Fig. 4. Energy-dispersive X-ray spectroscopy spectrum of RJA (a,b), MJA1 (c,d), and MJA2 (d,f) before and after adsorption.

presence of boron in the adsorbent. MJA1 and MJA2 also showed changes in elemental composition after adsorption, suggesting that the adsorbents selectively adsorbed certain types of organic compounds, leading to boron adsorption [34]. The EDX analysis provided quantitative evidence of the changes in elemental composition, which can help understand the adsorption process [48].

3.2. Batch adsorption studies

3.2.1. Effect of pH

The pH value significantly impacts the adsorption procedure and the amount of boron adsorbed in an H_3BO_3 solution [6]. Fig. 1a and b show the results of this investigation into the pH range of 2–12.5 for RJA, MJA1, and MJA2 adsorbents. Fig. 1a demonstrates that the quantity of boron adsorbed increased for both systems as the pH increased and reached a maximum at pH 6.5 for RJA and pH 7 for MJA1 and MJA2, respectively. In addition, Fig. 1a and b show that for RJA, boron adsorbed increased from 0.05 mg/g (3%) at pH 12.5 to 0.92 mg/g (61%) at pH 6.5. The uptake of boron rose for MJA1 and MJA2 from 0.19 mg/g (13%) to 0.94 mg/g (63%) and from 0.18 mg/g (12%) to 0.95 mg/g (63% removal efficiency), respectively, when the pH changed from 2 to 12.5 for a fixed starting boron content of 15 mg/L at equilibrium. Up to pH 7, the amount of adsorbed boron, q_t (mg/g), increased steadily with an increase in solution pH. After that, it dropped (Fig. 1a and b). In low ionic strength aqueous solutions, boric acid exhibits a pKa value of approximately 9.2. This value is essential as it signifies the pH at which boric acid initiates the deprotonation process, leading to the formation of borate ions. This transformation has a notable influence on the behaviour of boron species in solution and significantly impacts adsorption efficiency [49]. The findings indicated that the MJA1 and MJA2 had a higher ability to sorb boron than RJA. The highest level of boron adsorption has been recorded under circumstances of acidity and neutrality. The pH of the solution affects the functional groups present in

jering peel powder [28]. Based on previous studies, it has been observed that boron exists in an ionic form below a pH of 7.0. This characteristic enables easy absorption onto the adsorbent material by electrostatic interactions and binding with surface functional groups [29–31]. In general, it has been observed that functional groups present on the surface of the adsorbent tend to form bonds with hydrogen ions (H^+) at lower pH levels. This interaction between the functional groups and H^+ ions facilitates ions' attraction and subsequent adsorption [50]. The adsorption experiments conducted using RJA, MJA1, and MJA2 adsorbents demonstrated that the maximum boron adsorption was observed at pH 6.5 for RJA and MJA1, whereas MJA2 exhibited the highest adsorption at pH 7. The phenomenon described in the statement is accountable for the electrostatic connection between the boron and the surface of the jering powder, which has a negative charge [27]. At a high pH level, negative charges on the surface hinder the adsorption of boron due to the electrostatic attraction. However, at a low pH level, positive charges in the solution facilitate the adsorption of borate anions [12]. The pH at which the most significant boron adsorption occurs is seven because, at acidic pH, the oxide surfaces have a net positive charge, while at alkaline pH, they have a net negative charge [39,51]. The best efficacy of boron removal was seen at pH values of 6.5 and 7.0, which can be attributed to the presence of $B(OH)_3$ and the significant generation of $Fe(OH)_3$ [1,52]. In light of boric acid's pKa value, the drop in efficiency beyond pH of 7 can be explained. At pH values below 9.2, most of the boron species in the solution are uncharged boric acid, which allows for favourable electrostatic interactions and surface functional group binding between the boron species and the adsorbents [18]. As the pH increases beyond the pKa value, a significant portion of the boron species starts to deprotonate, forming negatively charged borate ions [49]. These negatively charged borate ions are less likely to interact strongly with the negatively charged surface of the adsorbent through electrostatic interactions [53]. As a result, adsorption efficiency decreases, leading to the observed drop in adsorption beyond pH 7. This study's results were consistent with those reported by Ku and Ismail [19], Kavak [21], Chaidir et al. [25], and Lata et al. [40] in their studies of boron removal using various adsorbents. In addition, the results were similar to those of Hurairah et al. [28], and Muslim and Said [29], who studied the jering peel as an adsorbent for various pollutants such as dyes and metal ions.

3.2.2. Effect of initial concentration

The initial concentration of boron in aqueous solutions affects the ability of jering peel powder to adsorb boron. The initial boron concentrations ranged from 2 to 20 mg/L, as represented in Fig. 1c and d, by which the effects of these concentrations on the boron adsorption can be evaluated. The results show that raw and modified jering powder's adsorption capacity (q_e) increased as the initial boron content rose. However, as the original boron content increased, the removal rate fell. As the initial boron concentration increased from 2 to 16 mg/L, boron's adsorption capability for RJA, MJA1, and MJA2 increased by 0.16 to 0.96 mg/g. These results imply that the initial boron concentration significantly influences raw and processed jering powder's ability to adsorb substances. Reducing the initial concentration of boron can lead to a quicker attainment of equilibrium concentration, resulting in higher absorption of boron [54]. The initial concentration of boron acts as the driving force to facilitate the mass transfer of boron between the solid and aqueous phases [36]. At higher initial boron concentrations with a constant dosage of adsorbent, the available adsorption sites on the adsorbent decrease, leading to a dependence of boron removal on the initial concentration [3]. This study reveals that treating jering peel powder significantly enhances its adsorption capacity compared to its untreated form. This improvement is attributed to removing impurities and interfering substances that hinder the active sites on the adsorbent surface [55]. The treated powder exhibits more available active sites, leading to heightened adsorption efficiency. This outcome underscores the transformative impact of treatment on adsorption capacity and highlights the potential of tailored refinement strategies for pollutant removal [2,6,19]. Drawing on existing literature to contextualize our findings, it becomes evident that the observations regarding jering peel powder align harmoniously with analogous studies exploring the removal of boron from contaminated water using diverse adsorbents. The concurrence of our outcomes with these established studies underscores the robustness and reproducibility of our findings, strengthening the credibility of our experimental conclusions [21,30,39,56].

3.2.3. Effect of adsorbent dose

The study utilized doses of RJA, MJA1, and MJA2 ranging from 0.2 to 1.5 g, as depicted in Fig. 1e and f, which clearly illustrate that as the adsorbent dose increases, the percentage of boron removal also increases. The findings indicated that the optimal percentage of boron removal was achieved with a dose of 1 to 1.5 g/L, resulting in a removal percentage of 61% to 71% (0.91–1.07 mg/g) for RJA, 62% to 66% (0.70–0.74 mg/g) for MJA1, and 65% to 69% (0.73–0.78 mg/g) for MJA2, as demonstrated in Fig. 1e and f. The study revealed that the percentage of boron removal increases as the adsorbent dose increases, as the corresponding adsorbent site area surface enlarges to facilitate adsorption due to the heightened active site of the adsorbent [39,57]. The salient observation emerged concerning the adsorption efficiency of boron within the specific dosage range of 1–1.5 g of adsorbent. Notably, a persistent and uniform trend was identified within this dosing interval, resulting in a graph characterized by conspicuous linearity. This intriguing behaviour strongly suggests an intricate interplay within this dosage range, potentially involving the modulation of ion exchange kinetics between the adsorbent and adsorbate [24]. The consistent adsorption efficiency exhibited at elevated adsorbent doses aligns with established principles, which posit that an elevated adsorbent quantity corresponds to a commensurate increase in the availability of adsorption sites, thereby fostering an intensified adsorption process [33]. The observed result is consistent with the adsorption concept, which states that an increased adsorbent dose creates more adsorption sites on the surface, where the adsorption

process occurs [1,25]. Conversely, when the total adsorbent dose is reduced, the surface of the adsorbent becomes saturated with ions, causing the concentration of these ions in the solution, which decreases the boron removal [28]. The results of this study are consistent with those reported by previous studies on using jering peels as an adsorbent for removing pollutants from water and wastewater [28–30]. Therefore, this suggests that jering seed peels have the potential to be a promising adsorbent for the removal of a variety of pollutants from aqueous solutions. Jering seed peels are a renewable and inexpensive material, making them a viable option for water and wastewater treatment [28–30], and were consistent with studies that used other adsorbents for removing boron from polluted water [21,53,58].

3.2.4. Effect of contact time

The rate at which adsorbents remove pollutants is crucial in determining the time needed for the system's adsorption effectiveness [33,59]. As evidenced by Fig. 4g and h, the temporal evolution of boron elimination is depicted. Notably, the removal efficiency of boron by RJA, MJA1, and MJA2 demonstrates a positive correlation with contact time. The elevated initial boron elimination rate is likely attributed to boron's rapid occupation of available active sites [22]. Following the initial phase, a gradual decline in boron elimination efficacy is observed beyond the 50-min mark, with minimal variations until the 120-min threshold. This phenomenon signals a potential avenue for future research, suggesting that investigations beyond 50 min may yield more profound insights into adsorption dynamics [39,58]. The accelerated removal rate of boron from the aqueous solution can be attributed to the abundance of active adsorption sites on the surface of RJA, MJA1, and MJA2 [27,28]. Studies have documented comparable observations involving diverse boron removal adsorbents [21,56,58,60]. The congruence between the adsorption behaviour of RJA, MJA1, and MJA2 and prior findings further supports the consistency of the experimental results [27,29,30]. In the context of the first 50 min, the swift adsorption of the adsorbate can be attributed to its rapid diffusion into the pores of RJA, MJA1, and MJA2, facilitated by their ample active sites. However, the subsequent stages necessitate a prolonged duration to adsorb boron, indicative of the limited active sites available for accommodating additional ions [17]. This phenomenon underscores the need to investigate means of enhancing active site availability, potentially through modifications to the adsorbent's structure or surface properties. Considering the broader landscape, the effective removal of low-level boron within 20 min aligns with findings in chelation studies that employ polymers for adsorption [61]. In contrast, equilibrium boron adsorption is reported to require 24 h [15]. RJA, MJA1, and MJA2 can remove boron from the aqueous phase due to their high adsorption efficiency and the short time required to reach equilibrium in our investigation.

3.2.5. Effect of temperature

Temperature plays a significant role in determining the effectiveness of an adsorbent in absorbing an adsorbate [39,59]. The temperature impact on boron adsorption by RJA, MJA1, and MJA2 was investigated at different temperatures between 25°C and 50°C, as depicted in Fig. 4i and j. The results showed that as temperature increased, the equilibrium adsorption capacity of boron onto both unmodified and modified jering powder decreased, attributed to a decrease in surface activity, indicating that the process of boron adsorption onto jering powder was exothermic [22,62]. The attractive interactions between the surface of the jering powder and boron also decreased with rising temperature, resulting in reduced sorption [63]. Consequently, boron in jering powder tended to change from the solid to liquid phase, making adsorption more effective at lower temperatures. Previous research has reported similar results on the adsorption of boron at different temperatures involving various systems [3,6,58,60]. The experimental findings revealed that the optimal adsorption capacity of RJA, MJA1, and MJA2 was most pronounced within the 25°C–30°C temperature range, as evident from Fig. 4i and j. his specific thermal interval exhibits a conspicuous amelioration in adsorption performance, with RJA evincing a substantial adsorption capacity of 0.88 mg/g (59%). Analogously, MJA1 and MJA2 manifest praiseworthy adsorption capacities of 0.93 mg/g (62%) and 0.87 mg/g (58%). This conspicuous augmentation in adsorption efficacy finds its underpinning in the augmented molecular mobility engendered by elevated temperatures, engendering more profound intermolecular interactions between the adsorbate and the adsorbent surface [11,64]. Nevertheless, it is imperative to acknowledge that an undue elevation in temperature may potentially elicit the undesired consequence of desorbing previously adsorbed boron from the adsorbent's surface, consequently culminating in a tangible contraction of the overall adsorption capacity [22]. This intricate interplay of temperature nuances and their consequential impact on adsorption dynamics underscores the significance of meticulous temperature management in the endeavour to optimize adsorption process efficacy.

3.3. Isotherm modelling

In the domain of isotherm modelling, a comprehensive understanding of adsorption dynamics mandates the incorporation of relevant parameters. This research systematically explored a variety of factors, including initial concentrations (ranging from 2 to 20 mg/L), pH (maintained at 6.5), contact duration (set at 120 min), temperature (maintained at 30°C), and adsorbent quantity (consistently set at 1 g per material). This methodical approach generated an extensive dataset, revealing the intricate interplay of these variables on adsorption patterns. Through this methodology, not only are diverse material applications acknowledged, but also the complete potential of synthetic endeavours is harnessed to elucidate potential utilities.

The Langmuir model often explains how a solute adheres to a solid surface [52]. This study uses the model to explain the boron adsorption onto RJA, MJA1, and MJA2. According to the model, adsorption occurs when solute molecules form a monolayer on the surface of the adsorbent [65]. The Langmuir parameters of RJA indicate excellent boron adsorption with a maximum absorption capacity (q_{max}) of

1.098 mg/g, a Langmuir constant (K_L) of 0.43, a separation factor (R_L) of 0.134, and a correlation coefficient (R^2) of 0.99. Therefore, these results suggest that RJA has a high affinity for boron. The R_L value is more than 0.1, indicating favourable adsorption. The model agrees well with the experimental data, as indicated by the R^2 value 0.99 in Table 1. For MJA1, q_{max} equals 0.75, K_L equals 2.069, R_L equals 0.03, and R^2 equals 0.91, as in Table 1. The Langmuir adsorption constant is 2.069, indicating the more effective adsorption. The relatively good fit of the Langmuir model to the experimental data is indicated by the R^2 value of 0.91. For boron absorbed by MJA2, the values of q_{max} equalling 0.72, K_L equalling 3.43, R_L equalling 0.02, and R^2 equalling 0.87, as in Table 1 and Fig. 5. The Langmuir adsorption constant is 3.43, suggesting that the adsorption is less effective than RJA and MJA1. The relatively good fit that the Langmuir model offers is indicated by the R^2 value of 0.87.

The Freundlich model assumes that adsorption happens through a surface with different adsorption energies and that the adsorption capacity increases as the solute concentration increases [62]. R^2, a parameter in the model with no units, is used to judge how well the model fits experimental data [66]. $1/n$ = 0.45, N = 2.21, K_f = 0.33, and R^2 = 0.84 for RJA. $1/n$ = 0.36, N = 2.77, K_f = 0.41, and R^2 = 0.87 for MJA1. $1/n$ = 0.35, N = 2.89, K_f = 0.43, and R^2 = 0.91 for MJA2 as in Table 1. All three adsorbents have $1/n$ values smaller than 1, which shows effective adsorption [67]. The MJA2 has a higher K_f value than the other two adsorbents, indicating a greater adsorption capacity [68]. The value of N is similarly higher for MJA2, showing that it has a higher adsorption ability at high boron concentrations. The Freundlich model adequately accounts for the experimental data, as seen by the R^2 values for RJA; it was fitted for the experimental data of MJA2 adsorbent as the R^2 value was 0.91. Raw jering powder's R^2 value, however, is lower than that of the other two adsorbents, demonstrating that it is less accurate than the other two.

Table 1
Parameter values of the isotherm models for the boron adsorption by the RJA, MJA1, and MJA2 adsorbents

Isotherm models	Parameters	RJA	MJA1	MJA2
Langmuir model	q_{max} (mg/g)	1.10	0.75	0.72
	K_L	0.43	2.07	3.43
	R_L	0.13	0.03	0.02
	R^2	0.99	0.92	0.87
Freundlich model	N	2.21	2.77	2.89
	$1/n$	0.45	0.36	0.35
	K_f	0.33	0.41	0.43
	R^2	0.84	0.87	0.91
Dubinin–Radushkevich model	q_m (mg/g)	0.80	0.80	0.83
	β (mol²/kJ²)	0.00	0.00	0.00
	E (kJ/mol)	1304.54	1575.43	1529.86
	R^2	0.95	0.82	0.88
Temkin model	B_T (J/mol)	0.20	0.17	0.16
	K_t (L/mg)	6.67	17.12	21.95
	R^2	0.89	0.79	0.83

The Temkin model is frequently used to describe the adsorption of a solute onto a solid surface [63]. A balance between the attractive forces between the solute molecules and the solid surface is assumed to characterize the adsorption process [29]. As in Table 1 and Fig. 6, the Temkin isotherm model calculates B_T = 0.20 J/mol and K_t = 6.67 L/mg for RJA, with an R^2 value of 0.89; this result reflects a modest heat of adsorption, as shown by the low K_t value. A significant correlation between the actual and predicted values and a high R^2 value indicates that the Temkin isotherm model well describes the data [69]. The model predicts a B_T value of 0.17 J/mol and a K_t value of 17.21 L/mg for MJA1, along with an R^2 value of 0.78, as in Table 1, suggesting a lower heat of adsorption than RJA, but significantly more binding energy as indicated by the higher K_t value. However, the model may not fit the data as well as it did for RJA, the lower R^2 score indicates that it still produces credible predictions [33]. The model predicts a B_T value of 0.16 J/mol for MJA2 and a K_t value of 21.95 L/mg with an R^2 value of 0.83, suggesting a lower heat of adsorption and even more significant binding energy than MJA1, as shown by the higher K_t value. With a significant correlation between the anticipated and actual values, the R^2 value shows that the model adequately fits the data.

The Dubinin–Radushkevich model, which describes how solutes adhere to solid surfaces, is frequently utilized [70]. The adsorbent's and adsorbate's physical and chemical characteristics administrate the adsorption process [71]. The model's output for RJA produced a high q_m value at 0.80 mg/g, indicating a high capacity for boron adsorption [38]. The calculation results indicate that the surface of RJA is energetically heterogeneous. It is clear from the high E value that boron and the adsorbent interact strongly [53]. Also, a high correlation between the predicted and observed values and the high R^2 value indicates that the model fits the data well. There was no discernible difference in the maximum adsorption capacity for MJA1, as indicated by the model's q_m value, which was similar to that for raw as in Table 1. The lower value denotes a surface less energetically heterogeneous than RJA, whereas the higher value of E denotes a more significant interaction [15] between the boron and the MJA1 and MJA2 surfaces. The model still makes logical predictions despite its lower R^2 value, suggesting it might not be as accurate a fit for the data as it was for RJA. In the case of MJA2, the model displayed a more significant value for q_m, indicating that the NaOH alteration enhanced the maximum adsorption capacity compared to RJA. A moderate interaction between boron and the MJA1 and MJA2 surface was suggested by the value of E, which was halfway between the values for RJA and MJA1. The value of E indicated an energetically heterogeneous surface. The model is well-suited to the data, as evidenced by the high R^2 value, which also shows that the predicted and observed values correlate well [72].

3.4. Kinetic modeling

In the context of kinetic modelling, the fundamental parameters of the experimental system play a crucial role in ensuring accurate and comprehensive analysis. In this study, the kinetic modelling was achieved based on a

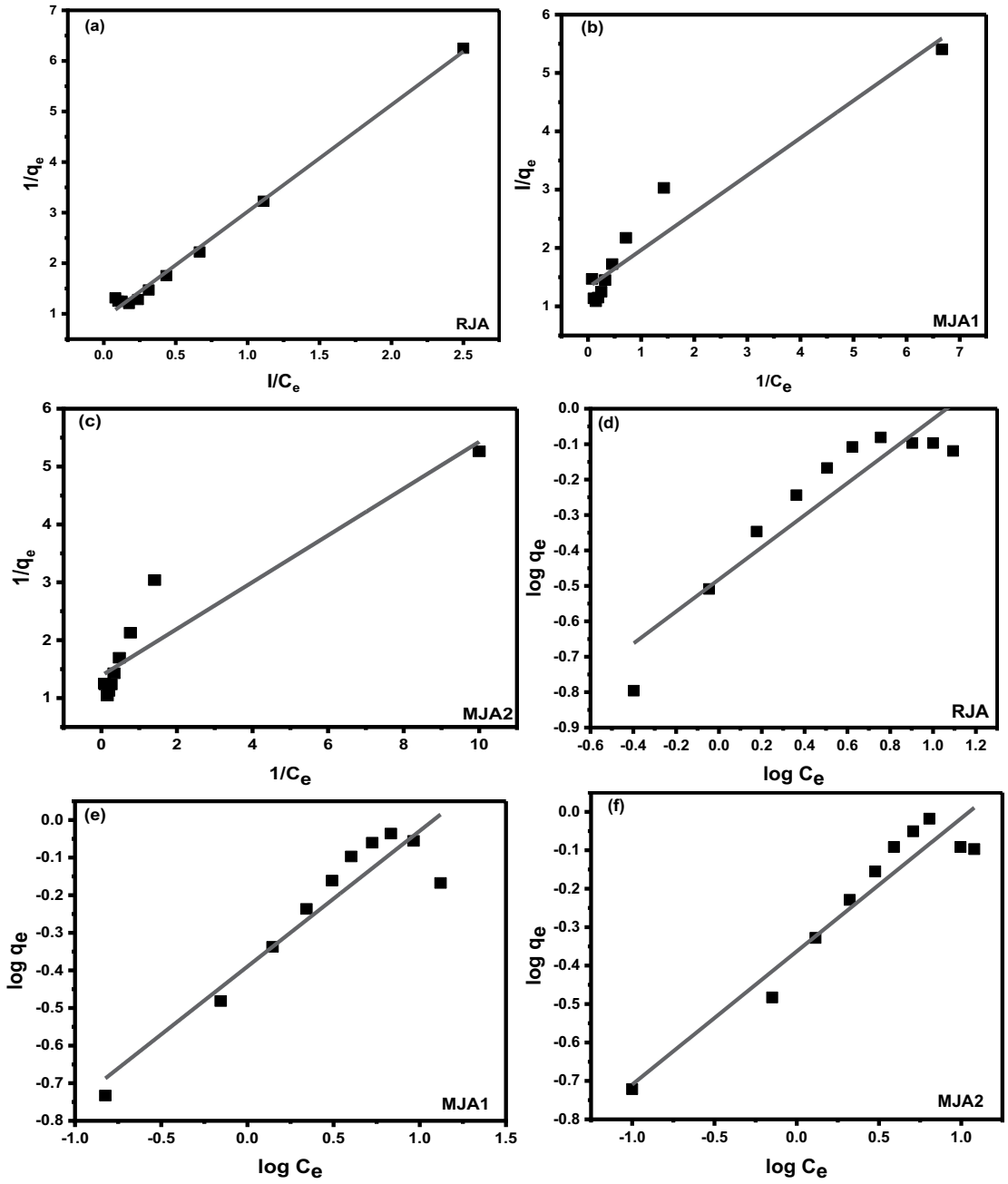

Fig. 5. Adsorption isotherm expression of Langmuir (a–c) and Freundlich (d–f) for boron adsorption by the RJA, MJA1, and MJA2.

comprehensive set of parameters encompassing various critical conditions. The system's pH was maintained at 6.5, while the contact time intervals were precisely controlled at 0, 10, 20, 30, 40, 50, 70, 90, 110, and 120 min. Furthermore, the initial concentration of the target compound was set at 15 mg/L, and an adsorbent dose of 1 g was employed. To facilitate a comprehensive understanding of the kinetic behaviour, the experiments were conducted at a consistent temperature of 30°C. This approach ensures a robust characterization of the adsorption process under a diverse range of conditions, mitigating the limitation of quoting a single '*K*' value for each material and thereby maximizing the utilization of the synthetic efforts invested in this study.

The pseudo-first-order model is a standard kinetic model for describing the adsorption behaviour of various pollutants onto various adsorbents where the adsorption rate is proportional to the number of free sites on the adsorbent surface [30,73]. This investigation tested boron adsorption on three types of jering powder, including RJA, MJA1, and MJA2. As in Table 2, the RJA's k_1 value was negative (–0.0064), and the correlation coefficient (R^2) was 0.98, indicating an excellent fit to the data that might be made even better. In contrast, the k_1 values for MJA1 and MJA2 were positive (0.00178 and 0.00197, respectively), indicating a good adsorption process, and the R^2 values were 0.98, showing exceptional data fit. MJA1 and MJA2 showed

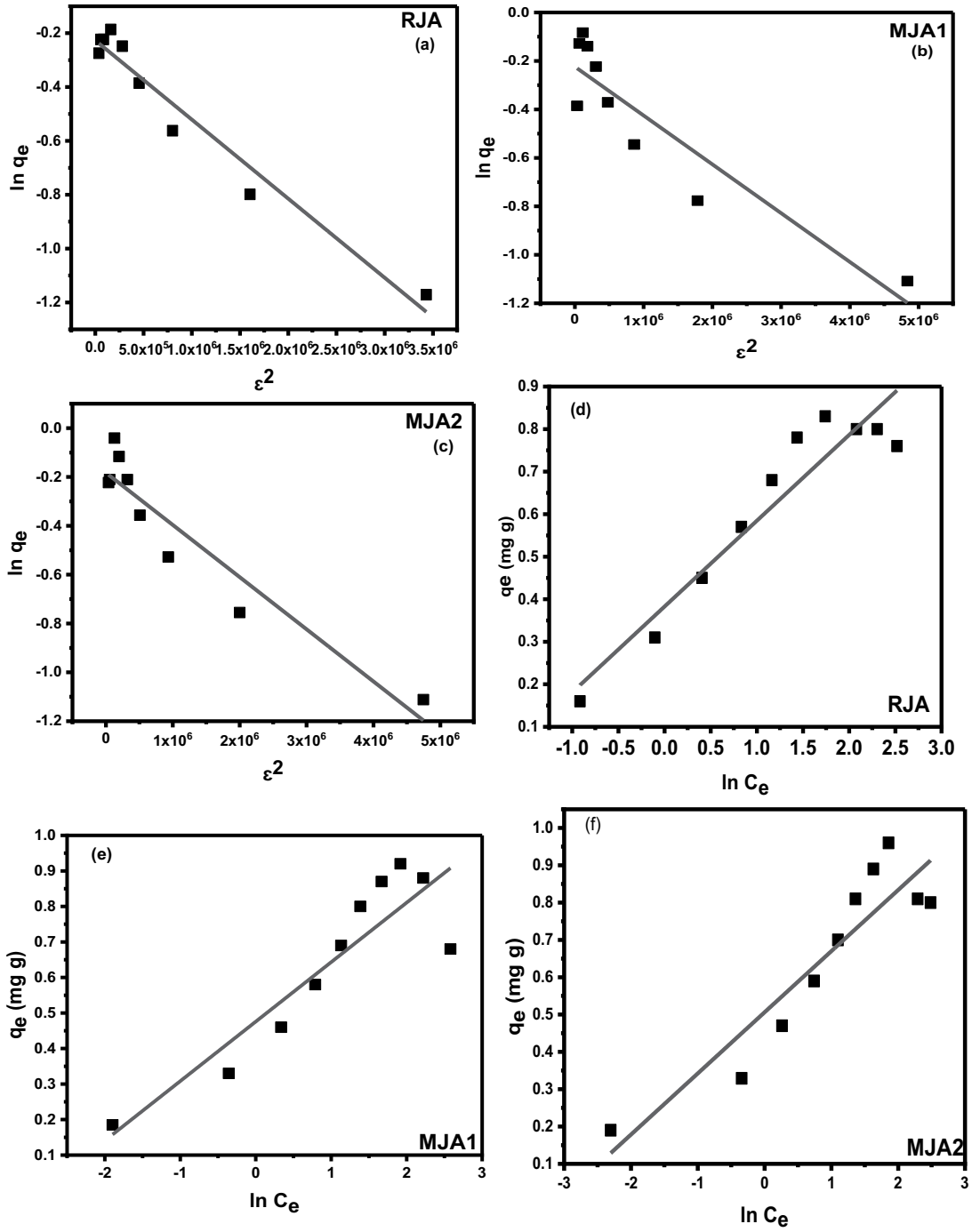

Fig. 6. Adsorption isotherm expression of Dubinin–Radushkevich (a–c) and Temkin (d–f) for boron adsorption by the RJA, MJA1, and MJA2.

relatively improved adsorption capacities than RJA, indicating that the modification process relatively improved the adsorption performance of the adsorbent [31]. In addition, the calculated q_e obtained from the model showed an agreement with the experimental q_e values as an indication of the fits of the model [70]. The positive values of k_1 for the modified adsorbents suggest that the adsorption process is favourable [74]. The high values of R^2 for all the adsorbents indicate a perfect fit for the data.

The pseudo-second-order model implies that the adsorption rate is directly proportional to the square difference between the available adsorption sites and the number of adsorbate molecules at any given moment and describes the adsorption of contaminants from wastewater using adsorbents [50,51,75]. As in Table 2, the q_e, k_2, and R^2 for RJA are 0.96 mg/g, 0.096, and 0.99, respectively. Furthermore, the MJA1 has a q_e value of 1.22 mg/g, a k_2 value of 0.022, and an R^2 value of 0.99. Additionally, q_e is 1.85 mg/g, k_2 is 0.015, and

Table 2
Parameter values of the kinetic models for the boron adsorption by the RJA, MJA1, and MJA2 adsorbents

Kinetic models	Parameters	RJA	MJA1	MJA2
Pseudo-first-order	q_e (mg/g)	0.46	1.24	1.27
	k_1	–0.01	0.00	0.00
	R^2	0.98	0.98	0.97
Pseudo-second-order	q_e (mg/g)	0.96	1.22	1.36
	q_e^2 (g/mg·min)	0.92	1.50	1.85
	k_2	0.10	0.02	0.02
	R^2	1.00	0.99	0.98
Intraparticle diffusion	K_{diff}	0.05	0.09	0.09
	C	0.40	0.06	0.00
	R^2	0.84	0.92	0.93
Elovich	α (mg/g·min)	6.02	3.51	3.21
	β (g/mg)	0.33	0.07	0.06
	R^2	0.95	0.98	0.99

R^2 is 0.98 for the MJA2. The high R^2 value shows that the experimental data and model fit well [73,74]. The fact that k_2 is positive means that the adsorption process is working well and that the adsorbate is adhering to the adsorbent's surface [30,70]. The model describes the adsorption kinetics of boron onto RJA, MJA1, and MJA2. As evidence of the model's fits, the calculated q_e produced from the model displayed an absolute agreement with the experimental results [31,33]. Also, RJA, MJA1, and MJA2 have a positive value for k_2, indicating that the adsorption process is successful and that these adsorbents can be utilized efficiently to remove boron from contaminated water.

According to the intraparticle diffusion model, the adsorption rate on adsorbent particles is controlled by the adsorbate's diffusion rate [72]. RJA's K_{diff}, C, and R^2 values are 0.048, 0.40, and 0.84, respectively, as in Table 2. The comparatively low R^2 value indicates that the experimental data and the intraparticle diffusion model do not match well. On the other hand, the positive K_{diff} value shows that the adsorption process is successful and the adsorbate is adhering to the surface of the adsorbent [71]. As shown in Table 2, A K_{diff} value of 0.085, C of 0.06, and R^2 of 0.92 are displayed by the MJA1, and the high value of R^2 denotes a good fit of the experimental data with the intraparticle diffusion model. Similar results were obtained with the MJA2, which had K_{diff} values of 0.092, C values of –0.003, and R^2 values of 0.93. A high R^2 value denotes a good match of the experimental data with the intraparticle diffusion model [73]. In both situations, the positive K_{diff} values signify a successful adsorption process in which the adsorbate is adsorbed onto the adsorbent surface. For the MJA1 and MJA2, the intraparticle diffusion model accurately predicts the boron adsorption kinetics, but not for the RJA. These adsorbents can effectively remove boron from contaminated water, as shown by the modified jering powder with $FeCl_3$ and NaOH's positive K_{diff} value and by the modest intercept C value, external mass transfer resistance has little effect on adsorption [30,33,69].

The Elovich kinetic model assumes that the adsorption process occurs through chemisorption and that there are a finite number of adsorption sites on the adsorbent surface [76]. As in Table 2, the RJA has α value of 6.02, β value of 0.33, and an R^2 value of 0.95. A high R^2 value denotes a strong fit with the model. The adsorbate is chemisorbed onto the adsorbent surface quickly, according to the high α value, and the low β value suggests the intense contact between the adsorbate and the adsorbent [77]. The MJA1 has an R^2 value of 0.98, a β value of 0.07, and an α value of 3.51; a high R^2 value denotes a strong match with the model. Low β values reflect a slow desorption process with the adsorbate tightly bonded to the adsorbent surface, while lower values signal a slower initial adsorption rate [78]. The MJA2 has an α value of 3.21, a β of 0.06, and an R^2 of 0.99, with a high R^2 value suggesting a good match with the model. The low β value indicates intense contact between the adsorbent and the adsorbate. Overall, the high value of R^2 for jering adsorbents indicates the effective removal of boron from polluted water [22]. For the effective removal of boron from water, the low β values for all three adsorbents indicate that the adsorbate is tightly attached to the adsorbent surface [53].

3.5. Thermodynamic modelling

Thermodynamic models predict the feasibility and spontaneity of chemical reactions, such as the adsorption of pollutants onto adsorbents [39,68,70]. The values of $\Delta G°$ at different temperatures indicate the feasibility of the adsorption process, whereas the negative $\Delta G°$ value indicates that the process is not spontaneous and thermodynamically favourable [39,67,79]. The Van't Hoff equation derived crucial thermodynamic insights regarding boron removal from aqueous solutions using RJA, MJA1, and MJA2, as shown in Fig. 7. The obtained intercept values (–30.66266 ± 3.3, –33.47431 ± 8, and –23.78579 ± 3.68077), upon multiplication by the gas constant (R), signify the entropy change ($\Delta S°$) of adsorbents modification, elucidating the thermodynamic favorability of the adsorption process in terms of entropy. Concurrently, the slope values (–8659.85116 ± 100, –9633.08844 ± 2494, and –6657.37662 ± 1147), similarly scaled by the gas constant (R), provide insight into the enthalpy change ($\Delta H°$) for each adsorbent, facilitating the determination of the endothermic or exothermic nature of the adsorption process concerning enthalpy. These data, complemented by the associated standard errors, significantly contribute to our comprehensive understanding of the energetics and feasibility of boron adsorption across RJA, MJA1, and MJA2. As shown in Table 3, the positive values of $\Delta G°$ indicate that the adsorption process is not spontaneous under standard conditions but can become spontaneous under non-standard conditions, meaning energy is required to initiate the adsorption process. However, the process can become energetically favourable as the boron concentration in the solution decreases or as the system's temperature changes [74,80]. For RJA, the $\Delta H°$ value is –72 kJ/mol, which indicates that the adsorption process is exothermic, releasing heat [6,77]. The negative $\Delta H°$ value also suggests that the

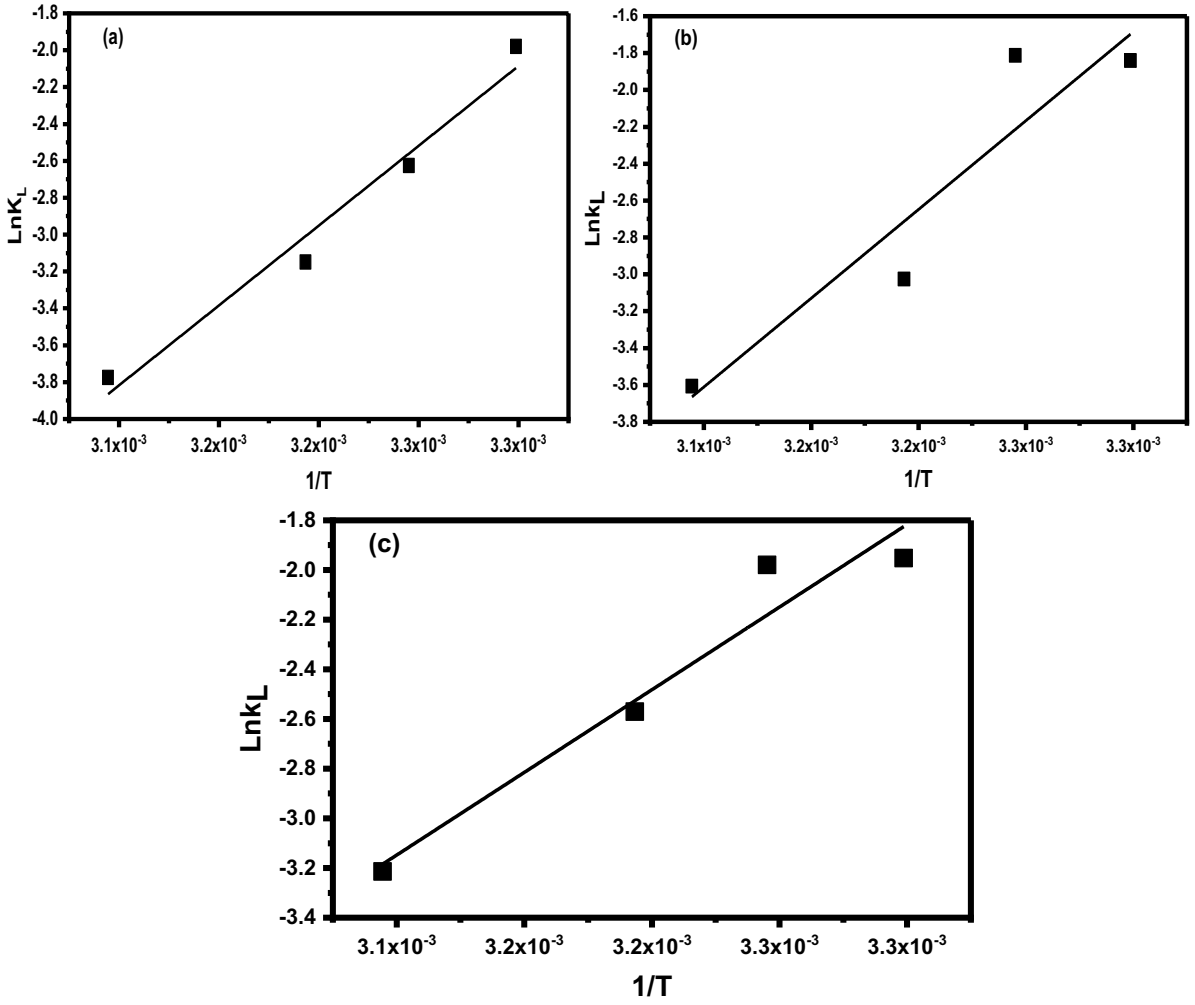

Fig. 7. The thermodynamic model plots of boron adsorption by the RJA (a), MJA1 (b), and MJA2 (c) adsorbents.

adsorption process is favourable, as it reduces the system's internal energy [50]. Also, the $\Delta S°$ value is –255 J/K·mol, and the negative $\Delta S°$ value implies that the adsorption process reduces the disorder or randomness of the system as the adsorbate becomes less random at the solid-solute interface during the adsorption process [52,81]. Despite this, the negative $\Delta S°$ value is offset by the negative $\Delta H°$ value, resulting in a positive $\Delta G°$ value and suggesting that the adsorption process is spontaneous [79,80,82]. The R^2 value of 0.96 suggests that the thermodynamic model fits the experimental data well for RJA. In addition, the $\Delta H°$ values indicate that the adsorption process of boron using MJA1 is exothermic, with energy being released [51,75]. Essentially, the decrease in the degree of disorder in the system is associated with the negative value of $\Delta S°$ [77]. The value of R^2 can determine the degree to which the model fits the data. As a result of the R^2 value, the model can be deemed moderately accurate. The boron adsorption onto MJA2 is exothermic and supported by the negative $\Delta H°$ value, indicating that heat is released during the process [3,51,75]. The negative $\Delta S°$ value further confirms a decrease in the system's randomness, which is expected in adsorption processes as well as an R^2 value of 0.92 suggests that the model fits the data. Generally, when the thermodynamic modelling shows negative values of $\Delta H°$ and $\Delta S°$ and a positive value of ΔG, it suggests that the adsorption process is energetically favourable, spontaneous, and exothermic, and reduces the disorder or randomness of the system [3,22,62].

3.6. Regeneration study of adsorbent

Fig. 8 illustrates the efficacy of regenerating jering peel adsorbents (RJA, MJA1, and MJA2) in removing boron from aqueous solutions. The graph indicates that the spent adsorbent has a reduced adsorption capacity compared to the fresh adsorbent. However, an interesting observation was made regarding boron removal rates. The rate of boron removal by RJA and MJA2, in which NaOH was used for regeneration, was comparable to that of boron adsorbed by MJA1, in which HCl was used for regeneration. Without the regeneration of adsorbents, the spent adsorbent lost its ability to remove boron in subsequent experiments after the initial adsorption cycle. However, the adsorption capacity increased during the first regeneration cycle but relatively decreased for the following cycles, as shown in Fig. 8. The adsorption process was reversible, and the acidic solution

Table 3
Thermodynamic parameters of the boron adsorption by the RJA, MJA1, and MJA2 adsorbents

Adsorbent	T (K)	K_a	ΔG (kJ/mol)	ΔH (kJ/mol)	ΔS (J/K·mol)	R^2
RJA	303	0.26	5	–72	–255	0.96
	308	0.16	6.8			
	313	0.05	8.2			
	323	0.03	10.1			
MJA1	303	0.14	4.6	–80	–278	0.82
	308	0.14	4.7			
	313	0.08	7.9			
	323	0.04	9.7			
MJA2	303	0.14	4.9	–55	–198	0.92
	308	0.07	5.1			
	313	0.04	6.7			
	323	0.02	8.6			

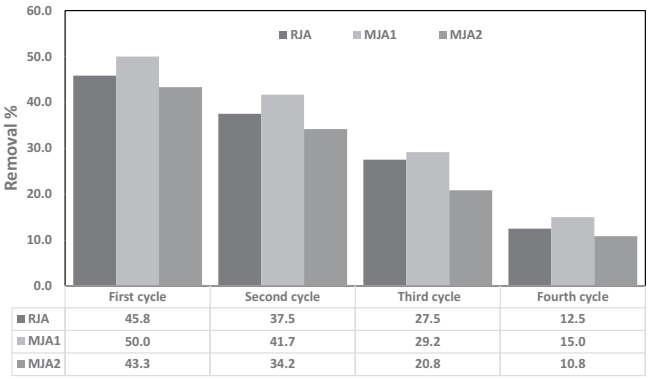

Fig. 8. Regeneration cycles of the jering adsorbents (RJA, MJA1 MJA2).

recovered the MJA1, while the alkaline solution recovered RJA and MJA2 to adsorb the boron. This phenomenon could be attributed to boron's dual acidic and basic properties in different chemical environments, resulting in electrostatic interactions with acidic and alkaline solutions and the consequent reversible reactions [83]. The cation can transform into a carbonyl base by adding NaOH to organic adsorbents. The polarity of oxygen can increase the acidity of the alpha hydrogens of carbonyl compounds, allowing for possible electrostatic attractions between an acid and a base [40,42].

4. Conclusion

This study employed jering peels as adsorbents, specifically RJA, MJA1, and MJA2, for boron removal from synthetic wastewater. The batch experiments for boron removal were conducted under optimal conditions, including pH, initial concentration, dosage, contact duration, and temperature, to attain the highest possible removal effectiveness. The FTIR spectra exhibited the presence of novel functional groups in the modified samples, suggesting the successful execution of the modification technique. The absence or reduction of peaks in the modified samples may be attributed to introducing, removing, or altering specific functional groups. Additionally, the FESEM analysis revealed alterations in the surface morphology of RJA, MJA1, and MJA2 before and following boron adsorption. These findings suggest that these materials possess promising characteristics as efficient adsorbents for removing boron from aqueous solutions. This study investigates the isotherm behaviour of boron adsorption using four different models. The results indicate that the adsorption of boron using RJA and MJA1 may be adequately described by the Langmuir model, while the Freundlich model provides a better fit for the boron adsorption data obtained with the MJA2 adsorbent. In addition, kinetic adsorption was carried out by four models that showed that the adsorption kinetics conforms to the pseudo-second-order model when the highest value of R^2 for all adsorbents compared to other kinetic models that also showed good fits of boron adsorption data in an indication that the chemisorption may be the rate-limiting step where electron exchange between the adsorbate and adsorbent involves valence forces. For the thermodynamic modelling, the negative values of $\Delta H°$ and $\Delta S°$ show that the boron adsorption is favourable, spontaneous, and exothermic and reduces the system's randomness as the adsorbate becomes less random at the solid-solute interface during the adsorption process. Jering peel adsorbents demonstrated good reusability in four consecutive adsorption–desorption cycles, making them potentially recyclable adsorbents for efficient boron removal from aqueous solutions. After lab-scale characterization through techniques, including FTIR, EDX, and FESEM, systematic optimization, model establishment for enhanced adsorption, effective boron regeneration methods, and proven durability through cycles, real-world boron removal tests confirm applicability and compliance, ensuring seamless commercial integration. Jering peel adsorbents have successfully scaled from lab to commercial.

Data availability

The datasets used and analyzed during the current study are available from the corresponding author upon reasonable request.

Conflict of interest

The authors declare no conflict of interest.

Acknowledgement

The authors express their gratitude to the Faculty of Science and Technology at Universiti Kebangsaan Malaysia for granting access to their research facilities and hosting the fellowship of the first author (GUP-2019-042). They also thank the International Institute of Education (IIE) Scholar Rescue Fund for providing the first author with a fellowship. Without the support of both institutions, the research would not have been possible.

References

[1] A. Abd Halim, A.F.A. Bakar, M.A.K.M. Hanafiah, H. Zakaria, Boron removal from aqueous solutions using curcumin-aided electrocoagulation, Middle East J. Sci. Res., 11 (2012) 583–588.

[2] E. Babiker, M.A. Al-Ghouti, N. Zouari, G. McKay, Removal of boron from water using adsorbents derived from waste tire rubber, J. Environ. Chem. Eng., 7 (2019) 102948, doi: 10.1016/j.jece.2019.102948.
[3] S. Alkhudhayri, O. Eljamal, I. Maamoun, R. Eljamal, Thermodynamic Effect on Boron Removal from Aqueous Solutions by MgAl Layered Double Hydrotalcite, Proceedings of International Exchange and Innovation Conference on Engineering & Sciences (IEICES), Kyushu University Institutional Repository, 2019, pp. 19–21.
[4] S. Bhagyaraj, M.A. Al-Ghouti, M. Khan, P. Kasak, I. Krupa, Modified *os sepiae* of *Sepiella inermis* as a low cost, sustainable, bio-based adsorbent for the effective remediation of boron from aqueous solution, Environ. Sci. Pollut. Res., 29 (2022) 71014–71032.
[5] Z.C. Çelik, B. Can, M.M. Kocakerim, Boron removal from aqueous solutions by activated carbon impregnated with salicylic acid, J. Hazard. Mater., 152 (2008) 415–422.
[6] A.Y. Goren, Y.K. Recepoglu, A. Karagunduz, A. Khataee, Y. Yoon, A review of boron removal from aqueous solution using carbon-based materials: an assessment of health risks, Chemosphere, 293 (2022) 133587, doi: 10.1016/j.chemosphere.2022.133587.
[7] E. Loizou, P.N. Kanari, G. Kyriacou, M. Aletrari, Boron determination in a multi element national water monitoring program: the absence of legal limits, J. fur Verbraucherschutz Leb., 5 (2010) 459–463.
[8] K. Rahmawati, N. Ghaffour, C. Aubry, G.L. Amy, Boron removal efficiency from Red Sea water using different SWRO/BWRO membranes, J. Membr. Sci., 423 (2012) 522–529.
[9] H. Polat, A. Vengosh, I. Pankratov, M. Polat, A new methodology for removal of boron from water by coal and fly ash, Desalination, 164 (2004) 173–188.
[10] X. Liu, C. Xu, P. Chen, K. Li, Q. Zhou, M. Ye, L. Zhang, Y. Lu, Advances in technologies for boron removal from water: a comprehensive review, Int. J. Environ. Res. Public Health, 19 (2022) 10671, doi: 10.3390/ijerph191710671.
[11] Z. Guan, J. Lv, P. Bai, X. Guo, Boron removal from aqueous solutions by adsorption–a review, Desalination, 383 (2016) 29–37.
[12] A. Halim, M. Hanafiah, M. Asmi, Z. Daud, Boron removal from aqueous solution using coagulation-flocculation with curcumin: a response surface methodology, J. Environ. Biol., 42 (2021) 750–755.
[13] H.C. Man, W.H. Chin, M.R. Zadeh, M.R.M. Yusof, Adsorption potential of unmodified rice husk for boron removal, BioResources, 7 (2012) 3810–3822.
[14] S. Singh, K.L. Wasewar, S.K. Kansal, Chapter 10 – Low-cost Adsorbents for Removal of Inorganic Impurities From Wastewater, P. Devi, P. Singh, S.K. Kansal, Eds., Inorganic Pollutants in Water, Elsevier, 2020, pp. 173–203.
[15] N. Öztürk, D. Kavak, Adsorption of boron from aqueous solutions using fly ash: batch and column studies, J. Hazard. Mater., 127 (2005) 81–88.
[16] H. Çelebi, İ. Şimşek, T. Bahadir, Ş. Tulun, Use of banana peel for the removal of boron from aqueous solutions in the batch adsorption system, Int. J. Sci. Environ. Technol., 20 (2023) 161–176.
[17] D. Kara, Removal of boron from aqueous solution by 2,3-dihydroxybenzaldehyde modified silica gel, Water Air Soil Pollut., 226 (2015) 1–9.
[18] S. Karahan, M. Yurdakoç, Y. Seki, K. Yurdakoç, Removal of boron from aqueous solution by clays and modified clays, J. Colloid Interface Sci., 293 (2006) 36–42.
[19] C.K.N.A.C. Ku, M.H.S. Ismail, Optimization of boron removal from aqueous solution via adsorption using composite beads of mangrove bark, alginate and zeolite, J. Chem. Eng. Ind. Biotechnol., 3 (2018) 1–12.
[20] J. Kluczka, W. Pudło, K. Krukiewicz, Boron adsorption removal by commercial and modified activated carbons, Chem. Eng. Res. Des., 147 (2019) 30–42.
[21] D. Kavak, Removal of boron from aqueous solutions by batch adsorption on calcined alunite using experimental design, J. Hazard. Mater., 163 (2009) 308–314.
[22] J. Wolska, M. Bryjak, Methods for boron removal from aqueous solutions—a review, Desalination, 310 (2013) 18–24.
[23] R.-j. Xu, X.-r. Xing, Q.-f. Zhou, G.-b. Jiang, F.-s. Wei, Investigations on boron levels in drinking water sources in China, Environ. Monit. Assess., 165 (2010) 15–25.
[24] M. Fildza, R. Rohmatullaili, A. Oktasari, Utilization of jengkol peel (*Pithecellobium jiringa*) as an adsorbent of iron metal, Walisongo J. Chem., 5 (2022) 130–135.
[25] Z. Chaidir, R. Zein, Q. Hasanah, H. Nurdin, H. Aziz, Absorption of Cr(III) and Cr(VI) metals in aqueous solution using mangosteen rind (*Pithecellobium jiringa* (jack) prain.), J. Chem. Pharm. Res., 7 (2015) 948–956.
[26] M.Y. Lubis, R. Siburian, L. Marpaung, P. Simanjuntak, M.P. Nasution, Methyl gallate from jiringa (*Archidendron jiringa*) and antioxidant activity, Asian J. Pharm. Clin. Res., 11 (2018) 346–350.
[27] S.N. Hurairah, N.S.M. Fahimi, A.A. Halim, M.M. Hanafiah, N. Nordin, N.A. Ab Jalil, Z. Daud, *Archidendron jiringa* seed peel extract in the removal of lead from synthetic residual water using coagulation-flocculation process, Sci. Asia, 49 (2023) 94–100.
[28] S.N. Hurairah, N.M. Lajis, A.A. Halim, Methylene blue removal from aqueous solution by adsorption on *Archidendron jiringa* seed shells, J. Geosci. Environ. Prot., 8 (2020) 128–143.
[29] A. Muslim, S.D. Said, Cu(II) ion adsorption using activated carbon prepared from *Pithecellobium jiringa* (*Jengkol*) shells with ultrasonic assistance: isotherm, kinetic and thermodynamic studies, J. Eng. Technol. Sci., 49 (2017) 472–490.
[30] M.R. Mohd Ramli, N.F. Shoparwe, M.A. Ahmad, Methylene blue removal using activated carbon adsorbent from jengkol peel: kinetic and mass transfer studies, Arabian J. Sci. Eng., 48 (2023) 8585–8594.
[31] T.K. Sen, S. Afroze, H. Ang, Equilibrium, kinetics and mechanism of removal of methylene blue from aqueous solution by adsorption onto pinecone biomass of *Pinus radiata*, Water Air Soil Pollut., 218 (2011) 499–515.
[32] M. Jalali, F. Rajabi, F. Ranjbar, The removal of boron from aqueous solutions using natural and chemically modified sorbents, Desal. Water Treat., 57 (2016) 8278–8288.
[33] A. Melliti, J. Kheriji, H. Bessaies, B. Hamrouni, Boron removal from water by adsorption onto activated carbon prepared from palm bark: kinetic, isotherms, optimisation and breakthrough curves modeling, Water Sci. Technol., 81 (2020) 321–332.
[34] N.U.M. Nizam, M.M. Hanafiah, E. Mahmoudi, A.A. Halim, A.W. Mohammad, The removal of anionic and cationic dyes from an aqueous solution using biomass-based activated carbon, Sci. Rep., 11 (2021) 1–17.
[35] T. Taşçı, G. Küçükyıldız, S. Hepyalçın, Z. Ciğeroğlu, S. Şahin, Y. Vasseghian, Boron removal from aqueous solutions by chitosan/functionalized-SWCNT-COOH: development of optimization study using response surface methodology and simulated annealing, Chemosphere, 288 (2022) 132554, doi: 0.1016/j.chemosphere.2021.132554.
[36] J. Kluczka, J. Trojanowska, M. Zołotajkin, Utilization of fly ash zeolite for boron removal from aqueous solution, Desal. Water Treat., 54 (2015) 1839–1849.
[37] A.O. Dada, J. Ojediran, A.A. Okunola, F. Dada, A. Lawal, A. Olalekan, O. Dada, Modeling of biosorption of Pb(II) and Zn(II) ions onto PaMRH: Langmuir, Freundlich, Temkin, Dubinin–Radushkevich, Jovanovic, Flory–Huggins, Fowler–Guggenheim and Kiselev comparative isotherm studies, Int. J. Mech. Eng. Technol., 10 (2019) 1048–1058.
[38] H.K. Afolabi, M.M. Nasef, N.A.H.M. Nordin, T.M. Ting, N.Y. Harun, A.A.H. Saeed, Isotherms, kinetics, and thermodynamics of boron adsorption on fibrous polymeric chelator containing glycidol moiety optimized with response surface method, Arabian J. Chem., 14 (2021) 103453, doi: 10.1016/j.arabjc.2021.103453.

[39] S. Vasudevan, J. Lakshmi, Electrochemical removal of boron from water: adsorption and thermodynamic studies, Can. J. Chem. Eng., 90 (2012) 1017–1026.
[40] S. Lata, P. Singh, S. Samadder, Regeneration of adsorbents and recovery of heavy metals: a review, Int. J. Sci. Environ. Technol., 12 (2015) 1461–1478.
[41] H. Patel, Review on solvent desorption study from exhausted adsorbent, J. Saudi Chem. Soc., 25 (2021) 101302, doi: 10.1016/j.jscs.2021.101302.
[42] J. Bayuo, M.A. Abukari, K.B. Pelig-Ba, Desorption of chromium(VI) and lead(II) ions and regeneration of the exhausted adsorbent, Appl. Water Sci., 10 (2020) 171.
[43] R. Ivan, C. Popescu, V. Antohe, S. Antohe, C. Negrila, C. Logofatu, A.P. Del Pino, E. György, Iron oxide/hydroxide–nitrogen doped graphene-like visible-light active photocatalytic layers for antibiotics removal from wastewater, Sci. Rep., 13 (2023) 2740, doi: 10.1038/s41598-023-29927-9.
[44] A.C. Heredia, M.M. de la Fuente García-Soto, A. Narros Sierra, S.M. Mendoza, J. Gómez Avila, M.E. Crivello, Boron removal from aqueous solutions by synthetic MgAlFe mixed oxides, Ind. Eng. Chem. Res., 58 (2019) 9931–9939.
[45] L. Sun, J. Huang, H. Liu, Y. Zhang, X. Ye, H. Zhang, A. Wu, Z. Wu, Adsorption of boron by CA@KH-550@EPH@NMDG (CKEN) with biomass carbonaceous aerogels as substrate, J. Hazard. Mater., 358 (2018) 10–19.
[46] A. Babkin, I. Burakova, A. Burakov, D. Kurnosov, E. Galunin, A. Tkachev, I. Ali, Adsorption of Cu^{2+}, Zn^{2+} and Pb^{2+} ions on a novel graphene-containing nanocomposite: an isotherm study, IOP Conf. Ser.: Mater. Sci. Eng., 693 (2019) 012045, doi: 10.1088/1757-899X/693/1/012045.
[47] A. Chowdhury, S. Kumari, A.A. Khan, M.R. Chandra, S. Hussain, Activated carbon loaded with Ni-Co-S nanoparticle for superior adsorption capacity of antibiotics and dye from wastewater: kinetics and isotherms, Colloids Surf., A, 611 (2021) 125868, doi: 10.1016/j.colsurfa.2020.125868.
[48] O.S. Bello, K.A. Adegoke, O.O. Akinyunni, Preparation and characterization of a novel adsorbent from *Moringa oleifera* leaf, Appl. Water Sci., 7 (2017) 1295–1305.
[49] E. Weidner, F. Ciesielczyk, Removal of hazardous oxyanions from the environment using metal-oxide-based materials, Materials, 12 (2019) 927, doi: 10.3390/ma12060927.
[50] S. Tariq, M. Saeed, U. Zahid, M. Munir, A. Intisar, M. Asad Riaz, A. Riaz, M. Waqas, H.M.W. Abid, Green and eco-friendly adsorption of dyes with organoclay: isothermal, kinetic and thermodynamic studies, Toxin Rev., 41 (2022) 1105–1114.
[51] S. Subramani, N. Thinakaran, Isotherm, kinetic and thermodynamic studies on the adsorption behaviour of textile dyes onto chitosan, Process Saf. Environ. Prot., 106 (2017) 1–10.
[52] H. Al-Zoubi, M. Zubair, M.S. Manzar, A.A. Manda, N.I. Blaisi, A. Qureshi, A. Matani, Comparative adsorption of anionic dyes (Eriochrome black t and Congo red) onto jojoba residues: isotherm, kinetics and thermodynamic studies, Arabian J. Sci. Eng., 45 (2020) 7275–7287.
[53] S. Bhagyaraj, M.A. Al-Ghouti, P. Kasak, I. Krupa, An updated review on boron removal from water through adsorption processes, Emergent Mater., 4 (2021) 1167–1186.
[54] T.T.H. Nguyen, Study of New Exchangers for Boron Removal From Water Containing High Concentration of Boron, Université De Toulouse, Ph.D. Dissertation, 2017.
[55] G.A. Wardani, L. Nuramalia, W.T. Wulandari, E. Nofiyanti, Utilization of jengkol peel (*Pithecellobium jiringa* (Jack) Prain) as lead(II) ions bio-sorbent with column method, Jurnal Kimia Sains dan Aplikasi, 23 (2020) 160–166.
[56] P. Remy, H. Muhr, E. Plasari, I. Ouerdiane, Removal of boron from wastewater by precipitation of a sparingly soluble salt, Environ. Prog., 24 (2005) 105–110.
[57] B.A. Fil, Isotherm, kinetic, and thermodynamic studies on the adsorption behavior of malachite green dye onto montmorillonite clay, Part. Sci. Technol., 34 (2016) 118–126.
[58] Y. Cengeloglu, A. Tor, G. Arslan, M. Ersoz, S. Gezgin, Removal of boron from aqueous solution by using neutralized red mud, J. Hazard. Mater., 142 (2007) 412–417.
[59] M.T. Yagub, T.K. Sen, S. Afroze, H.M. Ang, Dye and its removal from aqueous solution by adsorption: a review, Adv. Colloid Interface Sci., 209 (2014) 172–184.
[60] E.H. Ezechi, M.H. Isa, S.R. Bin Mohamed Kutty, Z. Ahmed, Electrochemical removal of boron from produced water and recovery, J. Environ. Chem. Eng., 3 (2015) 1962–1973.
[61] B.F. Senkal, N. Bicak, Polymer supported iminodipropylene glycol functions for removal of boron, React. Funct. Polym., 55 (2003) 27–33.
[62] S.-Y. Bang, J.-H. Kim, Isotherm, kinetic, and thermodynamic studies on the adsorption behavior of 10-deacetylpaclitaxel onto sylopute, Biotechnol. Bioprocess Eng., 22 (2017) 620–630.
[63] M. Erhayem, F. Al-Tohami, R. Mohamed, K. Ahmida, Isotherm, kinetic and thermodynamic studies for the sorption of mercury(II) onto activated carbon from *Rosmarinus officinalis* leaves, Am. J. Anal. Chem., 6 (2015) 1–10.
[64] N. Öztürk, T.E. Köse, Boron removal from aqueous solutions by ion-exchange resin: batch studies, Desalination, 227 (2008) 233–240.
[65] D. Balarak, J. Jaafari, G. Hassani, Y. Mahdavi, I. Tyagi, S. Agarwal, V.K. Gupta, The use of low-cost adsorbent (Canola residues) for the adsorption of methylene blue from aqueous solution: isotherm, kinetic and thermodynamic studies, Colloid Interface Sci. Commun., 7 (2015) 16–19.
[66] A. Bera, T. Kumar, K. Ojha, A. Mandal, Adsorption of surfactants on sand surface in enhanced oil recovery: isotherms, kinetics and thermodynamic studies, Appl. Surf. Sci., 284 (2013) 87–99.
[67] H.N. Bhatti, A. Jabeen, M. Iqbal, S. Noreen, Z. Naseem, Adsorptive behavior of rice bran-based composites for malachite green dye: isotherm, kinetic and thermodynamic studies, J. Mol. Liq., 237 (2017) 322–333.
[68] A. Darwish, M. Rashad, H.A. AL-Aoh, Methyl orange adsorption comparison on nanoparticles: isotherm, kinetics, and thermodynamic studies, Dyes Pigm., 160 (2019) 563–571.
[69] P. Maneechakr, S. Karnjanakom, Adsorption behaviour of Fe(II) and Cr(VI) on activated carbon: surface chemistry, isotherm, kinetic and thermodynamic studies, J. Chem. Thermodyn., 106 (2017) 104–112.
[70] S. Mustapha, D. Shuaib, M. Ndamitso, M. Etsuyankpa, A. Sumaila, U. Mohammed, M. Nasirudeen, Adsorption isotherm, kinetic and thermodynamic studies for the removal of Pb(II), Cd(II), Zn(II) and Cu(II) ions from aqueous solutions using *Albizia lebbeck* pods, Appl. Water Sci., 9 (2019) 1–11.
[71] D.R. Rout, H.M. Jena, Removal of phenol from aqueous solution using reduced graphene oxide as adsorbent: isotherm, kinetic, and thermodynamic studies, Environ. Sci. Pollut. Res., 29 (2022) 32105–32119.
[72] T.A. Saleh, Isotherm, kinetic, and thermodynamic studies on Hg(II) adsorption from aqueous solution by silica-multiwall carbon nanotubes, Environ. Sci. Pollut. Res., 22 (2015) 16721–16731.
[73] M.F. Onen, N.E. Aydin, O. Eksik, P. Demircivi, G.N. Saygili, Synthesis of graphene oxide for boron removal: equilibrium, kinetic and thermodynamic studies, Res. Square, (2022) 1–20.
[74] A. Olgun, N. Atar, Equilibrium, thermodynamic and kinetic studies for the adsorption of lead(II) and nickel(II) onto clay mixture containing boron impurity, J. Ind. Eng. Chem., 18 (2012) 1751–1757.
[75] P.B. Vilela, C.A. Matias, A. Dalalibera, V.A. Becegato, A.T. Paulino, Polyacrylic acid-based and chitosan-based hydrogels for adsorption of cadmium: equilibrium isotherm, kinetic and thermodynamic studies, J. Environ. Chem. Eng., 7 (2019) 103327, doi: 10.1016/j.jece.2019.103327.
[76] C. Cheung, J. Porter, G. McKay, Sorption kinetics for the removal of copper and zinc from effluents using bone char, Sep. Purif. Technol., 19 (2000) 55–64.
[77] L. Largitte, R. Pasquier, A review of the kinetics adsorption models and their application to the adsorption of lead by an activated carbon, Chem. Eng. Res. Des., 109 (2016) 495–504.
[78] J. Wang, X. Guo, Adsorption kinetic models: physical meanings, applications, and solving methods, J. Hazard. Mater., 390 (2020) 122156, doi: 10.1016/j.jhazmat.2020.122156.

[79] U.A. Edet, A.O. Ifelebuegu, Kinetics, isotherms, and thermodynamic modeling of the adsorption of phosphates from model wastewater using recycled brick waste, Processes, 8 (2020) 665, doi: 10.3390/pr8060665.
[80] Y.-S. Lim, J.-H. Kim, Isotherm, kinetic and thermodynamic studies on the adsorption of 13-dehydroxybaccatin III from *Taxus chinensis* onto sylopute, J. Chem. Thermodyn., 115 (2017) 261–268.
[81] A. Inyinbor, F. Adekola, G.A. Olatunji, Kinetics, isotherms and thermodynamic modeling of liquid phase adsorption of Rhodamine B dye onto *Raphia hookerie* fruit epicarp, Water Resour. Ind., 15 (2016) 14–27.
[82] M. Sulyman, J. Kucinska-Lipka, M. Sienkiewicz, A. Gierak, Development, characterization and evaluation of composite adsorbent for the adsorption of crystal violet from aqueous solution: isotherm, kinetics, and thermodynamic studies, Arabian J. Chem., 14 (2021) 103115, doi: 10.1016/j.arabjc.2021.103115.
[83] T. Ngulube, Removal of Cationic and Anionic Dyes From Aqueous Solution Using a Clay-Based Nanocomposite, University of Venda, Ph.D. Thesis, 2019.